

Petri Kaurola

# **LATERAL DIFFUSION ALONG CURVED LIPID BILAYERS**

Engineering and Science Faculty  
August 2019

## ABSTRACT

**PETRI KAUROLA:** Lateral diffusion along curved lipid bilayers

Tampere University of Technology

Master of Science thesis, 75 pages, 8 Appendix pages

August 2019

Master's Degree Programme in Science and Engineering

Major: Advanced Engineering Physics

Examiners: Prof. Ilpo Vattulainen, Dr. Matti Javanainen

Keywords: anomalous diffusion, lateral diffusion, membrane curvature, macromolecular crowding, molecular dynamics, Saffmann–Delbrück

Biomembranes are thin, encapsulating, lipid-based double-layered films prevalently crowded by membrane proteins, and the interactions between the lipids and the embedded proteins are an active field of study with vital relevance for cell biology and biomedicine. Many of these studies approximate lipid bilayers as flat planar structures, even though highly curved membranes, such as membrane tethers and buds, vesicles and liposomes, and in structures like cristae in mitochondria are prevailing. So far, it has been sufficient for scientists to answer simpler questions regarding biomembranes by focusing mainly on planar lipid bilayers. However, the advancements in experimental and computational methods allow and call for a deeper understanding also on how membrane curvature can affect the properties of membranes.

This thesis sheds light on the diffusion of proteins and lipids in curved lipid membranes. By presenting the first molecular dynamics simulations on the diffusion of transmembrane proteins in membrane tubes, the dynamics of the lateral diffusion in curved environments are studied in detail. The presented results highlight the importance of nanoscale curvature and compare the effect to macromolecular crowding, another currently confirmed factor related to lateral diffusion in lipid membranes. After a careful comparison between the results of this thesis and both experimental and computational work performed previously, pointers are given on how membrane curvature facilitated effects on lateral diffusion can be studied in the future.

## TIIVISTELMÄ

**PETRI KAUROLA:** Lateraalinen diffuusio kaarevilla lipidikaksoiskalvoilla

Tampereen teknillinen yliopisto

Diplomityö, 75 sivua, 8 liitesivua

Elokuu 2019

Teknisluonnontieteellinen koulutusohjelma

Pääaine: Teknillinen fysiikka

Tarkastajat: Prof. Ilpo Vattulainen, TkT Matti Javanainen

Avainsanat: anomaali diffuusio, lateraalinen diffuusio, kalvon kaareutuvuus, makromolekulaarinen ahtautuminen, molekyyldynamiikka, Saffman–Delbrück

Solujen kalvorakenteet ovat ohuita, kapseloivia, lipideistä koostuvia ja pääosin kalvo-proteiineilla ahdattuja kaksoiskelmuja, ja näiden proteiinien ja lipidien välisten vuorovaikutuksien ymmärtäminen on aktiivinen tutkimusala, jolla on sekä solubiologista että biolääketieteellistä merkitystä. Monet asiaan liittyvät tutkimukset approksimoivat lipidikaksoiskalvojen olevan laakeita tasokalvoja, vaikka voimakkaasti kaareutuneet kalvot, kuten esimerkiksi putkimaiset kalvokytkökset ja -rakkulat, vesikkelit, liposomit sekä soluelinrakenteet kuten mitokondrioiden kristat ovat valitsevia. Tähän asti tutkijoille on ollut pitkälti riittävää vastata yksinkertaisempiin solujen kalvorakenteita koskeviin kysymyksiin keskittymällä laakeisiin lipidikaksoiskalvoihin, mutta kokeellisessa ja laskennallisessa tutkimuksessa tapahtunut edistys mahdollistaa ja haastaa tutkimuksen keskittymään myös siihen, miten kalvon kaarevuus voi vaikuttaa kalvojen muihin ominaisuuksiin.

Tämä opinnäytetyö selkeyttää proteiinien ja lipidien mobiliteettia kaarevilla lipidikalvoilla. Tässä työssä esitetyt ensimmäiset kalvotuubeilla tehdyt transmembraaniproteiinien diffuusion keskittyvät molekyyldynamiikkasimulaatiot paneutuvat yksityiskohtaisesti lateraaliin diffuusion kalvoilla kaareutuneissa olosuhteissa. Työn tulokset korostavat nanoskaalan kaarevuuden merkitystä, jota verrataan makromolekulaariseen ahtautumiseen, joka on toinen jo tunnettu lipidikaksoiskalvojen lateraaliin diffuusion vaikuttava tekijä. Huolellisen tulosten tarkastelun ja aiempaan sekä kokeelliseen että laskennalliseen tutkimukseen tehdyn vertailun pohjalta tässä työssä ideoidaan mahdollisia jatkohankkeita kalvon kaarevuuden aiheuttamien vaikutusten selvittämistä varten.

## PREFACE

The work for this thesis was conducted in the biological physics research group lead by the Professor Ilpo Vattulainen, first in the physics department of Tampere University of Technology and later in Helsinki University, during the period between the end of 2015 and the middle of 2019. For a Master's thesis project, this research study that you are reading at the moment has been an exceptionally long process. This is partly due to my intervening exchange year in Japan, however, most of the challenges that this project has faced originate from the novelties related to it. The simulation structures I had to prepare were unique, and there were few tools that I was able to use to build them. It proved to be a difficult task to make my models stable and, because of the untraditional shape of my structures, most of the advanced analysis tools implemented in this work had to be made. Still, because of the resulting seemingly endless back and forth trial and error, the finished product, at least to me, is satisfying to both look at and to look back on in the end.

I have learned a lot during this project, but the single most important thing is perseverance. At times, it discouragingly seemed to me that if I ever was able to finish the project, the results would turn out to be dissatisfying, and all my efforts would be in vain. This could have very well been the case, since as always when doing exciting new science, you don't know what to expect, but in my case, I had hardly any reference that I would have been able to confidently compare my results to. This made it vexing to ponder whether my results were right at all. Despite this, from the very beginning of this project, I knew that I wanted to go through this alone as far as I could to prove my self-worth. In this, I feel I succeeded. The most important lesson one can learn from hardships such as this is that as long as one has the determination and motivation for progress, there are no concepts too complicated to be grasped or obstacles to be overcome that one wouldn't be able to achieve the unachievable.

Needless to say, I still did not write this thesis in solitude; above all else, it was assuring to be aware that I had always the possibility to consult my superiors, something I, of course, did take advantage of. The other examiner of this thesis and my main supervisor Matti Javanainen is an expert in his field of molecular dynamics simulations and the physics of biomembranes, and I tried to take his knowledge and teachings to heart the best I could. Every time after our discussions had ended, I

had a renewed zeal to explore further and to try to understand the analysis results that I had obtained. It was a privilege to be able to work with someone as driven, motivated, and intelligent person as him.

Like Matti, the other examiner of the thesis, my employer Professor Ilpo Vattulainen was a significant contributor to the success of this project. Before the project had even started, he could foresee the potential impact my thesis could have in scientific discussion, for it has been only quite recently that I have noticed emerging interest for nanoscale biomembrane curvature. Through consultations and throwing around thoughts and ideas, he has guided this project to answer its original research question, ultimately turning this thesis to be a coherent, thorough, and thought-provoking piece of science. After being my superior for several years, I have learned to appreciate his eagerness to be updated on the progress of the project while still temperately understanding to let his students take most of the responsibility for their work, making them learn of the experience. He is an instructor who truly wishes for what is best for his students, even if it would be contradicting his interests, and this is something that makes him truly stand out in my eyes.

Alongside Matti and Ilpo, I wish to thank all the members of Ilpo's research group and the people working close to it. The mind-stimulating discussions, the countless laughs, the boozy get-togethers, and boisterous travels are all something I will not cease treasuring. With a heavy heart, I will move on to new challenges after taking care of the rest of my projects in the group, but I am hopeful we will keep in touch. Also, my family deserves an honorable mention for they have done their part in helping me get this far in my studies. Yet, my advancements anything but stop here, and although I usually find radical changes in life, such as the end of this project, quite stressful, this time I feel differently; I have come to know that I have a lot to give and after realizing this, it has become clear that the end of this research project is, above all else, a new beginning for me.

Helsinki, 14th July 2019

Petri Kaurola

# Table of Contents

<b>1. Introduction</b>	<b>1</b>
<b>2. Membranes in Cells</b>	<b>4</b>
2.1 Structure and Function of Biological Membranes . . . . .	4
2.2 Crowding . . . . .	8
2.3 Membrane Curvature . . . . .	9
<b>3. Lateral Membrane Diffusion</b>	<b>15</b>
3.1 Brownian Motion in a Two-dimensional Space . . . . .	16
3.2 Anomalous Diffusion . . . . .	18
3.3 The Saffman–Delbrück Theory . . . . .	19
3.4 Displacements on a Cylindrical Surface . . . . .	22
<b>4. Molecular Dynamics Simulations</b>	<b>25</b>
4.1 Structures and Topologies . . . . .	25
4.2 Force Fields . . . . .	27
4.3 Martini Coarse-Grained Force Field . . . . .	30
4.4 Energy Minimization . . . . .	33
4.5 Equations of Motion . . . . .	34
4.6 Thermostats and Barostats . . . . .	35
4.7 Long-Range Interactions and Periodic Boundary Conditions . . . . .	38
<b>5. Model and Simulation Details</b>	<b>41</b>
5.1 Building the Tubular Bilayers . . . . .	41
5.2 Simulation Runs and Related Parameters . . . . .	45
5.3 Analysis Tools . . . . .	45
<b>6. Results and Discussion</b>	<b>48</b>
6.1 The Viscosity of Water . . . . .	48
6.2 Diffusion Coefficients and Exponents . . . . .	49

<i>TABLE OF CONTENTS</i>	VI
6.3 Longitudinal and Radial Diffusion . . . . .	54
6.4 The Extension to the Saffman–Delbrück . . . . .	60
<b>7. Conclusions</b>	<b>63</b>
<b>Bibliography</b>	<b>65</b>
<b>Appendix A: MSD and Anomalous Exponents</b>	<b>76</b>

## LIST OF ABBREVIATIONS AND SYMBOLS

$\beta_2$ AR	beta-2 adrenergic receptor
ATP	Adenosine triphosphate
CI	Confidence interval
CTRW	Continuous-time random walk
Cryo-EM	Cryogenic electron microscopy
DPPC	Dipalmitoylphosphatidylcholine
FCS	Fluorescence correlation spectroscopy
FLE	Fractional Langevin equation
FRAP	Fluorescence after photobleaching
GPCR	G protein-coupled receptor
MD	Molecular dynamics
MSD	Mean squared displacement
NVT	Canonical ensemble
NMR	Nuclear magnetic resonance
OmpG	Outer membrane porin G
PBC	Periodic boundary conditions
SPT	Single-particle tracking
VMD	Visual Molecular Dynamics
$\alpha$	Anomalous diffusion exponent
$\gamma$	Euler–Mascheroni constant
$\Delta t$	Displacement time
$\Delta t_{ts}$	Time step
$\epsilon$	The depth of the Lennard-Jones potential well
$\epsilon_0$	Vacuum permittivity constant
$\eta_{\text{eff}}$	Effective dynamic membrane viscosity
$\theta$	Angular displacement around a tube
$\theta_{ijk}^0$	Reference angle between three consecutively bonded particles
$\theta_{ijk}$	Angle between three consecutively bonded particles
$\mu_f$	Dynamic solvent viscosity
$\mu_m$	Dynamic membrane viscosity
$\xi_{ijkl}$	Dihedral angle formed by four bonded particles
$\xi_{ijkl}^0$	Reference dihedral angle formed by four bonded particles



$\sigma$	The equilibrium distance of the Lennard-Jones potential
$\tau_t$	Thermostat coupling time constant
$\tau_p$	Barostat coupling time constant
$\phi_{ijkl}$	Dihedral angle
$\phi_s$	Reference dihedral angle
$a$	Radius of a cylindrical inclusion
$b_{ij}$	Harmonic bond force constant
$c$	Principal curvature
$D$	Diffusion coefficient
$D_{sd}$	Saffman–Delbrück translational diffusion coefficient
$\mathbf{F}$	Force acting on a particle
$H$	Mean curvature
$h$	Membrane thickness
$h_n$	Maximum allowed displacement
$J$	Total curvature
$K$	Gaussian curvature
$k_\xi$	Improper dihedral angle force constant
$k_\phi$	Dihedral angle force constant
$k_B$	Boltzmann constant
$k_{ijk}^\theta$	Harmonic angle force constant
$k_{ij}^b$	Harmonic bond force constant
$L$	The length of a particle displacement
$L_{sd}$	Saffman–Delbrück length
$m$	Mass of particle
$P(x, t)$	Probability distribution function
$P$	Pressure matrix
$P_0$	Target pressure matrix
$q$	Electric charge
$R$	Radius of curvature
$\mathbf{r}$	Particle position in three-dimensional space
$r_{ij}$	Distance between two particles
$T$	Temperature
$T_0$	Temperature of a heat bath
$T_{\text{tot}}$	Total simulation time
$t$	Time
$V$	Potential energy
$V_a$	Harmonic angle potential

$V_b$	Harmonic bond potential
$V_C$	Coulomb potential
$V_d$	Periodic dihedral angle potential
$V_{id}$	Harmonic improper dihedral potential
$V_{LJ}$	Lennard-Jones potential
$\mathbf{v}$	Velocity of a particle
$x$	Particle position

# 1 INTRODUCTION

Cell membranes are an integral, interesting, and intensively researched branch of cell biology. For instance, by mediating the signaling of the cell with its surroundings, cell membranes are in a key position in determining all activity inside cells, making them and any related signaling proteins an attractive target for many drug-based treatments. Due to the vast complexity and small length and time scales of biological systems in general, the study of cells, and membranes in particular, have proven to be dauntingly challenging. Because it is expected that answering many of the unexplained questions dealing with cell membranes could greatly improve our understanding in illnesses tormenting human society, such as Alzheimer's disease, diabetes, and cancer, the motivation in exploring biological systems remains enduring.

Membrane curvature is one of the currently exciting themes dealing with biomembranes. Unlike what many simplified illustrations of planar lipid bilayers (the core of cell membranes) lead to believe, curvature in cell membranes is abundant and has been shown to be relevant for many essential cell processes. As an example, membrane curvature has been shown to sort G protein-coupled receptors, transmembrane signaling proteins embedded in the cell membrane [1], which has consequences on the function of these proteins dependent on the membrane environment. BAR domains, on the other hand, have been identified as highly conserved curvature-sensitive modules of several disease-associated proteins [2]. Curvature-mediated effects are not only limited to cell membranes, but concern all the other biomembranes inside the cell as well. ATP synthases, proteins in a pivotal role in the energy production of cells, are known to form long oligomeric rows at the tips of the cristae in the inner mitochondria membrane [3], which are known to be strongly curved membrane environments, further promoting the idea that membrane curvature should be a fundamental component when lipid-protein interactions are concerned.

Experimental techniques excel in finding and observing these thought-provoking cur-

vature mediated effects, but often lack in the ability to explain these phenomena. In order to examine how membrane proteins are influenced by the membrane curvature, one should be able to monitor these proteins in their natural condition at a nanometer spatial scale and in micro- to nanosecond temporal resolution. This is not usually possible in current experiments. Fortunately, the advancements in computing technology have allowed the development of computational tools, with which proteins can be simulated in their native environment at the required precision. In particular, molecular dynamics simulations have become an essential augmentation to traditional experiments [4], and by complementing each other these two approaches together are able to scrutinize lipid-protein systems, even when dealing with curved membranes.

In this study, a focus has been made on the dynamics of lipids and membrane-embedded proteins in curved lipid bilayers. By simulating tubular membranes with a controlled radius of curvature, it has been possible to isolate curvature mediated effects on the lateral diffusion, showing concretely how curvature is related to the diffusion of membrane particles. These are the first recorded molecular dynamics simulations which extensively tackle the transmembrane protein diffusion in highly curved membranes. Another topic related to diffusion, namely macromolecular crowding that is known to be a cause for the observed hindered anomalous diffusion [5, 6, 7, 8], has also been implemented in this work by creating simulations with varying protein concentrations, with an attempt to compare the crowding effects with the ones caused by membrane curvature.

The core of this thesis is comprised of seven chapters, which are complemented by an appendix presenting the graphs that support the discussions and results of this work. Following this introduction, the most important features of biomembranes are compactly briefed in chapter two. To expand it, macromolecular crowding and membrane curvature along with many publications related to them are reviewed, laying out some of the scientific background this study relies on. In chapter three, the focus sharpens to the lateral diffusion in membranes. The basics of two-dimensional normal diffusion are covered, after which anomalous diffusion in lipid membranes, an observed deviation from the idealistic diffusion, is discussed. Also, the approach of calculating displacement on cylindrical surfaces is explained, a quintessential step in studying diffusion with simulations.

In chapter four, the methodology of molecular dynamics simulations is presented.

Essentially, this includes an introduction to the theory of all the key components to consider when preparing simulations. Also, a special-type of modelling method called coarse-graining has been implemented in this study and thus is given attention in the discussion. Following this, the applied tools, methods, parameters, and other simulation and analysis details are given in chapter five.

The sixth chapter gathers the results of the thesis based on the data in the appendix, and this is where the main discussion of the study is done. The validity of the results is contemplated and a comparison with previous studies will be made along with comments on them. The final seventh chapter summarizes the key findings of this thesis. Based on the reflection on earlier research and current knowledge, feasible future steps in membrane curvature studies are conceptualized.

## **2 MEMBRANES IN CELLS**

To ultimately understand the lateral diffusion of proteins and lipids in lipid bilayers mimicking biological conditions, it is first fruitful to review biomembranes in general. We start by examining their structure, composition, and function, after which we pay attention to the crowding effects caused by high protein concentrations present in living cells. Finally, we will provide examples of ways how to quantify curvature and of biologically relevant situations where membrane curvature is significant.

### **2.1 Structure and Function of Biological Membranes**

All information in this section can be found from the reference [9] unless mentioned otherwise.

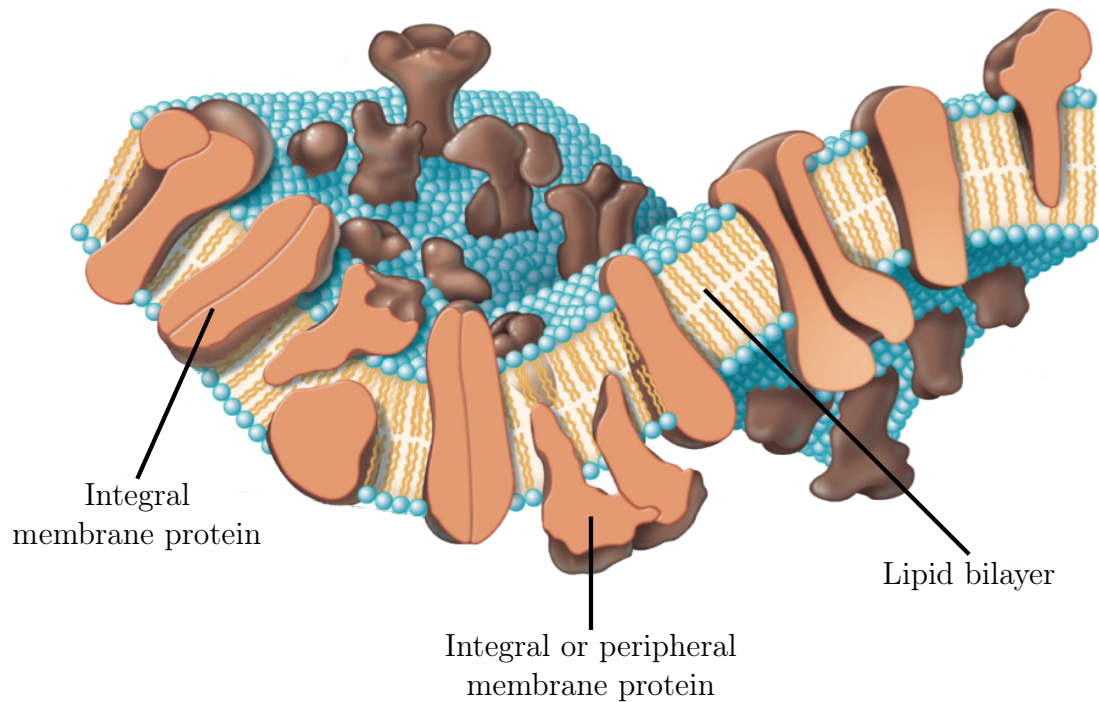
Cells are the smallest individual living units of which all known life forms are formed. Although the appearance, size, habitat, and specialized functions of cells vary greatly, on a fundamental level they are microscopic assemblies of biomolecules within which biochemical reactions take place unceasingly. Some of these reactions aim to utilize exterior energy sources, such as nutrients, chemicals, or radiation, while some of them employ this energy accompanied by other biomolecules. These reactions are the foundation of cell metabolism, which enables interaction with the surrounding environment as well as the preservation of these reactions facilitating cell's survival. This desire for a cell to thrive and to preserve the continuity of life manifests in cell motility, growth, reproduction, adaptation, and the intake of nutrients as well as the export of cell waste.

Most of the fundamental chemical reactions occur inside the cells, within an aqueous solution called cytoplasm. It is a concentrated mixture of chemicals, molecules, macromolecules, and cell organelles that carry out specific yet crucial tasks such as energy production. The cytoplasm is enclosed and separated from the environment by a thin and elastic membrane structure known as the plasma membrane or the cell

membrane. The isolation of the cytoplasm is discriminatory, meaning that although in principle the plasma membrane is impermeable — particularly to larger molecules — some specific molecules are either free to flow through it or they are actively transported from one side of the plasma membrane to the other. This selective transportation enables cells to conserve the cytoplasm but it simultaneously allows signaling molecules, nutrients, and waste flow through the membrane in a controlled manner.

The main two constituents of plasma membranes, as well as other biomembranes, are molecules called lipids and proteins. Lipids form the bulk of the membrane, a lipid bilayer, in which integral membrane proteins are embedded. Lipid bilayers tend to be approximately five nanometers in thickness and the different layers or leaflets in the bilayer may be asymmetrical in composition, as is in the case of plasma membranes. In animal cells, lipids and membrane proteins comprise almost equally the total mass of the membrane; however, since proteins can be significantly larger than lipids, the number of proteins in a bilayer is only a fraction of the number of lipids. In addition to lipids and proteins, carbohydrates are present in a coating called the carbohydrate layer adjacent to the noncytosolic side of plasma membranes as glycosylations in the proteins and lipids, forming compounds such as glycolipids, glycoproteins, and proteoglycans. The carbohydrate gives protection against mechanical and chemical damage and it makes the cell distinguishable to other cells as a result of unique arrangements of sugar monomers in branched chains. A schematic and highly simplified illustration of a cell membrane can be seen in Figure 2.1 [10].

Membrane proteins can be divided by either their structure or function. As depicted in Figure 2.1, integral membrane proteins can be thought to be structural protein components of the membrane being embedded in the membrane irreversibly, either on one leaflet or both. Polytopic integral membrane proteins, also known as transmembrane proteins, can directly interact in the case of plasma membrane with both the cytosol and the extracellular matrix. Peripheral membrane proteins on the other hand are reversibly associating with only one of these sides without penetrating the membrane. Alternatively, and perhaps more prominently, membrane proteins can be categorized according to their functional roles. Enzymes are proteins which catalyze biochemical reactions and while they do not need lipid bilayer by definition, some of them — such as transferases in the endoplasmic reticulum — are attached to it since the bilayer can provide an essential interface for the catalysis. Transporter proteins



**Figure 2.1** A model figure illustrating a cropped section of a simplified plasma membrane. Integral membrane proteins are embedded irreversibly in an elastic lipid bilayer and can be further divided into polytopic (transmembrane) or monotopic depending on whether they span the lipid bilayer completely or associate only with one leaflet. Peripheral membrane proteins interact with the membrane without being embedded in it and are able to disassociate from it. Glycosylations and all the details of the proteins have been left out for clarity. Modified from the reference [10].

and channels enable selective transportation of molecules through membranes while receptor proteins deliver signals into and out from the cell. Anchor proteins enhance the physical rigidity of the membrane by covalently bonding to macromolecules on either side of the membrane. An example of this is the spectrin meshwork, in which spectrin and actin proteins are linked to anchor proteins and make up a net of protein strings on the membrane surface. This structure improves yield strength and allows active bending and reshaping of the membrane. Also, the meshwork compartmentalizes proteins to restricted regions on the membrane, limiting the accessible surface area membrane proteins can diffuse to on the membrane.

Although proteins are the main source of the biological activity in cells, lipids are the foundation of the biomembranes, for without them cytosol could not be separated from the surroundings and membrane proteins would remain without structural



support. What makes many lipids excellent constituents for membranes is the fact that in the water phase they form membrane structures spontaneously. This is because lipids are amphipathic molecules, consisting of hydrophilic head groups and hydrophobic hydrocarbon tails, and when in contact with the water phase, the lipids assemble in two stacks of leaflets where hydrophilic headgroups face the water face and the ends of hydrocarbon chains face each other, thus, forming a bilayer. This minimizes the interface between hydrophobic hydrocarbons and the water phase in order to maximize entropy. Due to the hydrocarbons, lipid bilayers are highly hydrophobic, making it unfavorable for water-soluble molecules to passively diffuse through it. Though the spontaneous formation of membrane structures can seem as if entropy is decreasing due to the ordering of lipids, for the whole system entropy is increasing since the water molecules can freely form hydrogen bonds between each other. As a consequence, maintaining or even building lipid assemblies out of individual lipid molecules requires no energy, which is from the cell's point of view highly profitable. It is worth noting, though, that lipid bilayers are just one of the possible energetically favorable membrane structures along with, for example, micelles, liposomes, and — as more relevant for this thesis — membrane tubes.

Besides being the body of biomembranes, many of the lipids are in direct contact with the embedded membrane proteins. These lipid-protein interactions affect the stability of the protein structures, and ultimately the functionality of the interacting proteins [11]. It remains still debatable, whether specific and long-lasting lipid interactions or the dynamical effects of the membranes as a whole are the dominant effects governing protein functionality, but for now, it can at least be said that both are important. For example, in the case of G protein-coupled receptors, beta-2 adrenergic receptor ( $\beta_2$ AR), a model example of GPCRs, has been shown to have strong binding pockets for cholesterol along its surface [12], while it is also known that the lipid composition and ordering affects the partitioning of  $\beta_2$ AR in a lipid bilayer [13]. Related to this, it has been suggested that biomembranes contain transient nanoscale domains called lipid rafts [14], which would due to different lipid compositions and ordering effects be distinguishable from the rest of the bulk, further promoting the heterogeneity of membranes. Though they have not been explicitly proven to exist, they would have relevance for lipid-protein interactions due to the sensitivity and proximity of the proteins towards the lipids.

One more point worth mentioning about lipids is the plethora of different lipid types. The possible different backbones and head groups (when they can be unambiguously

identified), the lengths of hydrocarbon chains and the locations of double or even triple bonds in the case of unsaturated lipids are all variables that make the list of potentially existing lipids almost limitless. Commonly, lipids are divided based on their backbones (for example glycerol, phosphoglycerol, or a type of a sphingoid) and their head groups (in the case of phosphoglycerols, for example, choline, ethanolamine, or serine) [15]. Some lipids are very common, such as phosphatidylcholines, which in mammalian cells account for more than half of all the lipids, while most lipids are found in much smaller concentrations, usually fulfilling a role in signaling pathway. When faced with the complexity of the different lipid types, it is tempting to try to focus only on a few most prevalent and universal lipid types, but even the differences between two very similar lipids can be relevant; any abnormalities in the expression of a specific lipid can be a cause for a disease, which tells us that in the case of lipids, details matter [16].

## 2.2 Crowding

As mentioned already in the earlier section, proteins and carbohydrates are major components in addition to lipids in a biological membrane. In particular, the presence of proteins and other macromolecules is a major contributor to the properties of membranes, but only for the last few decades the abundance of large entities in membranes, known as crowding, has been acknowledged as a notable factor. Theories exist saying that by being packed with macromolecules, cells are able to enhance slow processes limited by state-transitions because proteins can interact for longer times this way, while faster processes related to diffusion are slowed down by the obstructing macromolecules [17]. Regardless of the benefits, it is important to recognize that partly due to the crowding effect, the experimental results acquired in dilute *in vitro* conditions are not directly transferrable to biological conditions, since these two environments differ drastically.

The first experiments on crowding focused on testing the Saffman–Delbrück theory (discussed further in section 3.3) at the beginning of the eighties [18, 19]. Though it could not be explicitly proven whether the theory holds or not, the results about the hindering effects of protein crowding on lateral diffusion were indisputable. A few years later, the first simulations attempting to understand protein crowding were made, by using simple Monte Carlo models focusing on diffusion in the presence of mobile obstacles [20], and the findings were similar. In the nineties, the differences of enzyme kinetics in dilute and crowded conditions also gained interest [21], and

though no diffusion models, which would directly take crowding into account, had been proposed, theoreticians also acknowledged the relevance of crowding [22].

During the last ten years, crowding studies have gained further popularity from many aspects; in addition to more traditional single-particle tracking (SPT) or other methods related to diffusion like fluorescence correlation spectroscopy (FCS), atomic force microscopy has been used to study motions of unlabelled membrane proteins [23], new extensions to diffusion models introducing correlated membrane protein motion and protein crowding in the means of effective membrane viscosity have been suggested [24], and several molecular dynamics and mesoscopic simulations of both proteins and lipids have revealed various effects. These include anomalous diffusion effects lasting for milliseconds [8], explicit quantifications of crowding-mediated impacts on diffusion coefficients, the hindrance of lipid diffusion with respect to the distance from obstructing membrane proteins [25], and the hindrance of protein diffusion with lengthy water-soluble parts [26]. All the proceedings in the crowding studies have provided enough information for comprehensive reviews, highlighting the role of crowding in membrane deformation and intracellular trafficking, the formation of transient lipid-protein assemblies and the slowdown of diffusion [5].

Recently with simulations, crowding has been shown to promote non-Gaussian displacement probability distributions [27], bringing diffusion in crowded conditions further away from normal Brownian motion regime, and more complicated and heterogeneous crowded membrane simulation models have been made to incorporate both protein crowding and protein size effects proposed by the Saffman–Delbrück theory [28]. At the moment, it appears that when moving from dilute to concentrated physiological conditions (from 400:1 to 50:1 lipids (per leaflet) to protein ratio), the protein mobility decreases gradually but non-linearly, and the decrease can be even an order of magnitude, particularly with the smaller sized proteins. This does not take into account, for example, restricting spectrin meshworks, water-soluble domains of proteins or heterogeneity of lipid bilayers, not to mention membrane curvature, suggesting that even more drastic slowdowns caused by crowding are possible.

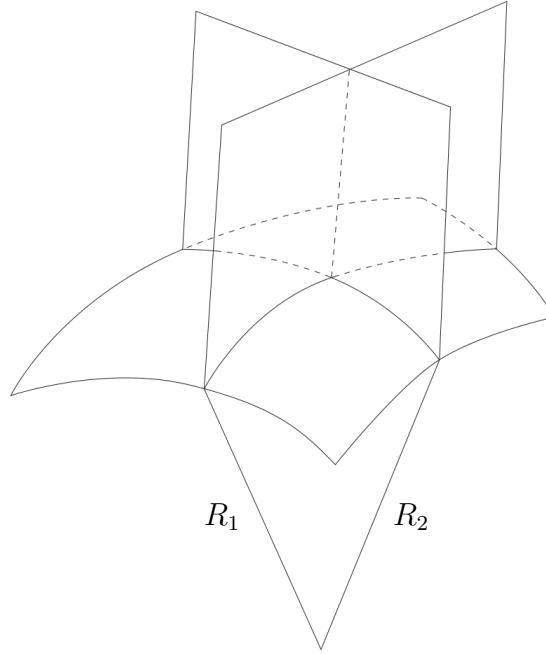
## 2.3 Membrane Curvature

Lipid bilayers are viscoelastic, meaning that they can bend and stretch like rubber would, but instead of being solid they are resilient viscous fluids. Syrup could

be thought to be an analogous substance with similar properties, however, lipid bilayers are quasi-two-dimensional (surfaces with a non-zero thickness) and have a lot of compositional variety, making such comparison misleading. Being nanoscale structures, they are in the constant bombardment of thermal fluctuations, which inevitably causes the membranes to deform even when in energetically favorable structures like planar bilayers or liposomes. Therefore, unlike what is usually shown in cell biology textbooks, curvature is abundant in cell membranes. Besides, cellular mechanisms make great use of this membrane moldability, allowing for example endocytosis, exocytosis, and cell division, promoting the importance of the curved structures in lipid bilayers as an active player rather than a thermal consequence [29].

Mathematically, curvature can be characterized extensively. For starters, it is important to understand that the curvature of a two-dimensional surface usually varies depending on the direction on the surface. At an arbitrary point of the surface, called the center of curvature, two circles can be drawn so that their curves are superimposed with the membrane tangent and they orthogonally cross each other at the center of curvature. The circles form so-called normal and osculating planes. The radii of these circles,  $R_1$  and  $R_2$  (the line along the principal normal from the center of curvature to the center of the circle of curvature or the osculating circle) define in one way the curvature at the center of curvature. This is illustrated in Figure 2.2. Though these circles can be drawn in any direction, they are by convention drawn along the principal axes, which specify the directions where the curvature is the largest and the smallest. Further details are found from reference [30].

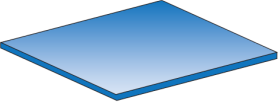
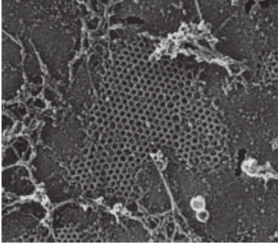

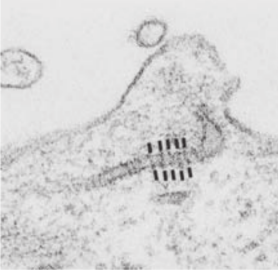
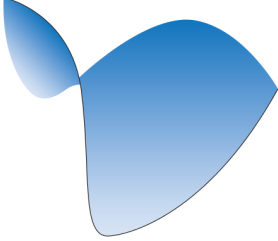
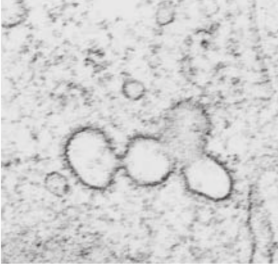
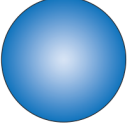
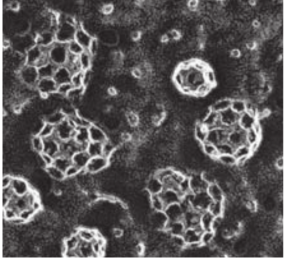
Since for planar membranes the radii of curvature are infinite, it is mathematically more appropriate to work with the respective inverses, the principal curvatures, defined as  $c_1 = R_1^{-1}$  and  $c_2 = R_2^{-1}$ . The values and signs of principal curvatures specify what kind of shape the surface has at the center of curvature, and if the values remain the same throughout the surface, the shape of the object is completely described. Alternatively, the total curvature  $J$  and the Gaussian curvature  $K$  can be used for compact surface shape description, defined as  $J = c_1 + c_2$  and  $K = c_1 c_2$ . Figure 2.3 shows different surface shapes and the parameters describing them, along with examples where such shapes are present in cell biology. Also, another useful and powerful measurable for the membrane curvature is the mean curvature  $H$ , where the curvatures at a center of curvature are integrated over all the angles around the center on the surface. This can be used when studying whether a protein can induce membrane curvature upon interaction, as done in the reference [32].



**Figure 2.2** An illustration of the quantification of membrane curvature. At the center of curvature, two planes perpendicular to the orthogonal tangents on the membrane plane, drawn in the directions of the maximum and minimum curvature, specify the principal axes. The radii of circles drawn on top of these planes, which align with the membrane surface at the center of curvature, are the radii of curvature  $R_1$  and  $R_2$ , and the inverses of these are the principal curvatures  $c_1$  and  $c_2$ . The figure is modified from reference [31].

Tubular membrane structures are of particular interest in this study. They exist in cell organelles such as Golgi apparatus, mitochondria, and endoplasmic reticulum being involved in intra- and extracellular exchange processes, spanning from the radius as small as tens of nanometers to the lengths as long as several hundred microns [33, 34, 35]. Also, the axons extending from neurons, interconnecting to other neurons with synapses to form neural circuits, are myelin covered membrane tubes with a radius as small as one micron [36]. Tubes can be made and observed experimentally and they are structurally more stable compared to unsupported vesicles, which makes them appropriate for studying membrane curvature mediated effects on membrane dynamics.

Only quite recently, membrane curvature in nanoscale has become accessible for experimental methods to study. In the early years of the current millennium, it was discovered by pulling membrane tubes from liposomes that membrane curvature ordered membranes by sorting lipids [37]. Also, proof had started to accumulate

		$c_1$	$c_2$	$J$	$K$	
a)		0	0	0	0	
b)		+	0	+	0	
c)		+	-	0	-	
d)		+	+	+	+	

**Figure 2.3** Principle, total, and Gaussian curvatures of different surface shapes accompanied by examples from cell biology. a) Planar membranes have no curvature at all. The flat bilayers to which clathrin lattices, bundles of proteins interacting with actin, retain their planar shape. b) Cylindrical membranes have curvature only along one principal axis. Such membranes can be found for example when dynamin proteins polymerize on the membrane surface, creating a dynamin coated tubular neck during bud formation in the endocytic pathway. c) Saddles have curvature in both directions of principal axes, but the surface is concave in one direction and convex in the other. Saddles are present in the necks of budding vesicles. d) Spheres have uniform curvature in all directions. Occasionally, small vesicles can take a form close to spherical, but clathrin cages made *in vitro* keep their spherical shape. The figure is modified from reference [31].

that proteins were able to induce membrane curvature [31]. At the same time, both experimentalists and theoreticians had an emerging interest in understanding lipid dynamics in curved membranes [38, 39]. In particular, interestingly from the point of view of this thesis, a theory extending the Saffman–Delbrück diffusion model to curved membranes like membrane tubes was presented by Rob Daniels and Matthew Turner [40] (discussed further in chapter 3). The first experimental study focusing on membrane dynamics, done by a research group led by Prof. Patricia Bassereau, where it was possible to effectively control membrane curvature in the range of tens of nanometers, was done by using SPT on tubular membranes [41]. The study supported the well-established hydrodynamic Saffman–Delbrück diffusion model and its later extensions by Daniels and Turner by showing that a smaller tube radius strongly hindered the lateral diffusion of transmembrane proteins on curved membranes compared to flat ones, though the used tracing particles had relatively large domains in the water phase and it was not possible to monitor diffusion around the tube axis. An extension to this study, where the possible method biases were addressed and tube radius was increased to hundreds of nanometers by using neurites, showed that the curvature effects on lipid dynamics on a larger scale were almost diminished [42]. When using these results to understand living cells, it is noteworthy that by studying other factors of membrane dynamics, such as bending modulus or friction, the dynamics between synthetic lipid bilayers and plasma membranes were known to differ, especially in the presence of cytoskeleton [43], so the results acquired so far were not universally applicable. Regardless, at this point it seemed that by ranging the tube radius from tens to hundreds of nanometers, a logarithmic increase in the lipid and protein diffusion coefficient in the longitudinal direction could be observed in the systems from highly curved tubes to effectively almost planar ones. For lipids, the diffusion along a planar bilayer could be approximately three times faster, whereas for proteins a five-fold boost was detected.

In recent years, the interplay between proteins and membrane curvature has become more evident. Similarly to lipids, curvature was experimentally shown to sort proteins as well [44]. So far, as according to the Saffman–Delbrück theory, the protein size was thought to be the major factor in protein mobility, however, the shape of protein was also found to have an effect on the membrane dynamics, possibly through membrane tension [45]. From the membrane’s point of view, a random-walk-free computational study suggested that the protein sorting could be a solely geometrical effect in tubes, although many contributed factors such as diffusing particle size and tube radius dependent hydrodynamics were not considered.

A state-of-the-art piece of knowledge about the relation between curvature and protein sorting is the finding that adenosine triphosphate (ATP) synthase dimers in inner mitochondrial membrane induce membrane curvature, further proving that ATP synthase dimers self-assemble at the edges of cristae into rows [46]. Because curvature effects on the nanoscale have become relevant in experimental cell biology to this extent, it has also become reasonable to attempt to find accurately the magnitude of these effects.



### 3 LATERAL MEMBRANE DIFFUSION

Diffusion is a physical process caused by thermal energy which drives the motion of small particles in liquid or gas phase substances. Because of diffusion, separate constituents of solutions or gas mixtures can blend spontaneously, giving rise to entropy in agreement with the second law of thermodynamics. In biological systems, it is well-suited to be employed as an effective and effortless mean of transportation of molecules in cells and is thus critical for the overall cell function, even though the thermal fluctuations are random. Mathematically, diffusion can be formulated in several different ways and it may be applied to many fields beyond cell biology. One of the more practical approaches is to observe a particle of interest for a relatively long time and follow its trajectory. This is known as single-particle tracking and has been implemented in the work of this thesis.

Although diffusion occurs usually in three dimensions, the particles can be physically restricted in a way that reduces the degrees of freedom for translation. For example, in contrast with traditional fluids and gases, transmembrane proteins embedded in a lipid bilayer can only diffuse along the dimension parallel to the membrane surface, since the dissociation of the proteins into the water phase is not energetically favorable. This two-dimensional movement is better known as lateral diffusion. This is how lipids and proteins can distribute evenly on lipid bilayers, at least when obstructions such as cytoskeleton or the oligomerization of proteins are not considered.

In this chapter, the ideal theory behind Brownian motion in two-dimensions is elucidated, after which one of the main focuses of the thesis — the Saffman–Delbrück theory — is introduced, along with some relevant experiments, improvements, and discussions found in the literature. Finally, a derivation is made for how the displacements of particles on a curved, tubular membrane surface can be calculated, relevant to the practical approach of this thesis.

### 3.1 Brownian Motion in a Two-dimensional Space

Brownian motion is known as the diffusion of a single micro- or nano-scale particle in a solution of considerable smaller particles acting as a fluid environment. First discovered experimentally by Robert Brown in the 19th century [47], it was formulated by Albert Einstein almost one hundred years later by applying a random walk model, also known as the Wiener process [48, 49]. It is a solution to the Einstein equation of diffusion or essentially the Fick's second law:

$$\frac{\partial}{\partial t}P(x, t) = D \frac{\partial^2}{\partial x^2}P(x, t), \quad (3.1)$$

where the factor  $D$  corresponds to the *diffusion coefficient*, a value describing the rate of diffusion,  $x$  is the particle position,  $t$  is time, and  $P(x, t)$  is a probability density function for the particle position, a function of both space and time [50]. Next, two-dimensional Brownian random walk will be derived in accordance with reference [47], in which a more thorough derivation is available.

Let us first derive a formula for a one-dimensional random walker and then extend it to a two-dimensional case. A particle takes a step  $k_j L$  where  $k_j$  has an equal chance of being either 1 or -1 and  $L > 0$  is a constant step length. This describes a situation, where at each time step a random walker takes a step of length  $L$  to either to the left or to the right. At step  $j$ , the position is  $x_j$  and if the initial position is set to be  $x_0 = 0$ , we get  $x_1 = k_1 L$ ,  $x_2 = x_1 + k_2 L$  and ultimately as a general rule  $x_j = x_{j-1} + k_j L$ .

On average, this yields the total displacement to be zero; if the particle has an equal chance of either moving to the left or to the right, after  $N$  steps the mean of the displacements results in the particle's initial location. However, by calculating the mean of displacements squared after  $N$  steps, we get

$$\langle (x_N)^2 \rangle = \langle (x_{N-1} + k_N L)^2 \rangle = \langle (x_{N-1})^2 \rangle + 2L \langle x_{N-1} k_N \rangle + L^2 \langle (k_N)^2 \rangle. \quad (3.2)$$

The last term equals  $L^2$ , because  $\langle (k_N)^2 \rangle$  equals 1. The middle term equals 0, since no square is taken of the displacement in that term, resulting in an average displacement of zero. Therefore, according to the acquired formula after each step the square displacement increases by  $L^2$ . In other words, after  $N$  steps the mean

squared displacement can be written as

$$\langle (x_N)^2 \rangle = NL^2. \quad (3.3)$$

Now, if we let the random walker move for time  $t$ , the number of steps  $N = t/\Delta t$ , where  $\Delta t$  is the duration of a single step, which is considered to be constant. Let us declare diffusion coefficient as  $D = \frac{L^2}{2\Delta t}$ . By replacing  $N$  in equation (3.3) by  $N = \frac{2Dt}{L^2}$ , we get

$$\langle (x_N)^2 \rangle = 2Dt. \quad (3.4)$$

This is the diffusion law of a one-dimensional random walker: the mean squared displacement (MSD) after  $N$  steps is linearly proportional to the time  $t$ . In reality, random movement does not necessarily happen in steps as this model assumes, but since the length of the step can be arbitrarily chosen to be infinitesimally small, the movement can be thought to be smooth and fluent instead of discrete, modeling the translation of real particles more accurately.

When deriving the MSD for a two-dimensional random walker, two approaches can be taken. The displacements can simply be thought to be the diagonals of squares, where the sides of the squares are  $x$ - and  $y$ -direction displacements (constants). The diagonals are of length  $\sqrt{2}L$ , and when following the earlier derivation, a diffusion law is obtained, where the proportionality is doubled compared to the one-dimensional case:

$$\langle (x_N)^2 \rangle = 4Dt. \quad (3.5)$$

Alternatively, the displacements in  $x$  and  $y$  directions can be considered separately:

$$\langle (\mathbf{r})^2 \rangle = \langle (x_N)^2 + (y_N)^2 \rangle = \langle (x_N)^2 \rangle + \langle (y_N)^2 \rangle, \quad (3.6)$$

leading to the same derivation as before and ultimately to the same result of  $\langle (\mathbf{r}_N)^2 \rangle = 4Dt$ .

Similarly, with the help of the random walker model, MSD can be derived in 3 dimensions. One might mistakenly argue, that the three-dimensional MSD model should be employed instead of the two-dimensional model in this work; after all, although lipid bilayers are two-dimensional surfaces, in the case of a membrane tube

the bilayer is connected to itself, forming a three-dimensional object. While this is true, the proteins diffuse only in two-dimensional space, along the membrane surface. Three-dimensional movement would require that the transmembrane protein could detach from the tube altogether. This will be further elucidated in section 3.4.

## 3.2 Anomalous Diffusion

The Brownian motion discussed so far describes a theoretical case where the mean squared displacement of a diffusing particle is directly proportional to the elapsed time. In reality, this is not necessarily the case: instead of being a perfect linear curve, MSD can behave as a power law with respect to time, where the curve may experience both momentary decreases (sub-diffusion) or increases (super-diffusion) in the slope of the curve. This behavior is known as anomalous diffusion.

At the beginning of the millennium, when it had become clear that the effects of macromolecular crowding on diffusion could not be neglected [51, 52], more attention was brought into finding more accurate models describing diffusion in crowded environments [7], although the first signs of non-linear diffusion time-dependence were from as early as 1926 [53], and first simulations from the early nineties [54]. Traditional experiments — while doable and even successful — proved to be a challenging way to study diffusion mechanisms [6, 55], but on the other hand, molecular dynamics simulations were capable of capturing all the relevant dynamic details of particle motion, either supporting or rejecting the prevalent anomalous diffusion models [56, 57]. It had become apparent that the measurement results of mean squared displacement and diffusion coefficients were significantly time-dependent.

Many suggested models trying to explain anomalous diffusion exist, examined extensively in several review papers during the last decade [7, 50, 58], to which the only common factor is the acknowledgment of the non-Brownian form of the mean squared displacement curves, resulting from the central-limit theorem not applying to anomalous diffusion. This is argued to be because — unlike what simple diffusion models assume — diffusing particles experience persistent displacement correlation. Therefore, the main goal for the developed diffusion models is to include these correlations so that anomalous diffusion is achieved. For example, fractional Langevin equation (FLE) — an extension to the ordinary Langevin equation, which models particle diffusion as a combination of a driving force and a stochastic white noise resulting from thermal fluctuations — includes Gaussian noise correlations so that

anomalous diffusion is produced. Another example is the continuous-time random walk (CTRW) model, where unlike in the regular Brownian motion, particle displacement lengths follow a given probability distribution, and the same can hold for the jump rate of the displacements. With this modification, anomalous diffusion is achieved when for example the jump rate distribution is defined so that the characteristic waiting time between jumps (the mean of the jump rate distribution) is mathematically infinite. The FLE model has acquired support from molecular dynamics simulations [57], but so far, universal conclusions cannot be made.

Though this thesis is not aiming to support or disprove any of the diffusion mechanism models, some focus on the anomalous diffusion behavior is given for two reasons. Firstly, in this work, it has been acknowledged that diffusion coefficients acquired by approximating the motion to be Brownian is generally invalid, and by observing the anomalous diffusion exponent  $\alpha$  in the power-law form of the two-dimensional Brownian motion, given by the equation

$$\langle \text{MSD} \rangle = 4Dt^\alpha, \quad (3.7)$$

it can be said how much trust can be put on the acquired diffusion coefficients. Secondly, by comparing the diffusion exponent  $\alpha$  between curved and crowded systems, it is possible to tell if curvature could promote subdiffusion as strongly as crowding is known to.

### 3.3 The Saffman–Delbrück Theory

When studying cellular functions, liquid phase systems tend to be easier to examine compared to membrane systems. After all, membranes are surrounded by an aqueous solvent, making them nanoscale two-phase systems which are far more convoluted compared to plain liquid solvent. This complexity applies specifically to the membrane proteins, because they have both hydrophobic and hydrophilic surfaces, and they tend to be more flexible than proteins in an aqueous solvent [59]. It is also not appropriate to isolate the membrane proteins from their native membrane environment, since this procedure would most likely affect the protein conformation of interest. Due to the difficulty of dealing with membrane proteins experimentally, all alternative methods of providing insight into unresolved properties of membrane proteins are welcome.

In the pioneering work by Philip Saffman and Max Delbrück, published in the seventies, a hydrodynamic model describing the dynamics of cylindrical membrane inclusions were introduced as an attempt to find a two-dimensional analogue to the famous Stokes–Einstein equation describing the three-dimensional diffusion of a Brownian particle [48, 49, 60, 61]. The result was the Saffman–Delbrück theory, which assumed a solid cylinder embedded in an incompressible hydrodynamical continuum (the membrane) of equal height as the cylinder (protein), surrounded by much less viscous solvent (for example, cytoplasm). Also, the model assumes a no-slip boundary condition, meaning that the velocity or the current of the surrounding continuum reaches zero at the surface of the inclusion due to friction. The equations for translational and rotational diffusion are given separately, but from the point of view of this research, only the prediction for the translational diffusion is of particular interest:

$$D_{\text{sd}} = \frac{k_{\text{B}}T}{4\mu_{\text{m}}h} \left[ \ln \left( \frac{2L_{\text{sd}}}{a} \right) - \gamma \right], \quad (3.8)$$

where  $D_{\text{sd}}$  is the Saffman–Delbrück translational diffusion coefficient,  $k_{\text{B}}$  is the Boltzmann constant,  $T$  is the temperature,  $\mu_{\text{m}}$  is the dynamic membrane viscosity,  $h$  is the thickness of the membrane,  $L_{\text{sd}} = h\mu_{\text{m}}/2\mu_{\text{f}}$  is the Saffman–Delbrück length, where  $\mu_{\text{f}}$  is the viscosity of the surrounding fluid,  $a$  is the radius of the cylindrical inclusion, and  $\gamma$  is the Euler–Mascheroni constant ( $\approx 0.57721$ ). The benefit of using a notation for Saffman–Delbrück length comes from the approximation of the model, which requires that the inclusion radius  $a$  should be significantly smaller than the Saffman–Delbrück length. In practice, inclusions are of the same size as the membrane thickness, and thus, in theory, Saffman–Delbrück can describe the motion of nanoscale particles. Still — if proven to be correct — the theory could be helpful in estimating the sizes of membrane-embedded inclusion by observing the dynamics of the inclusion with relatively simple microscopy.

A few years later, the theory had inspired experimental research and was initially supported by fluorescence after photobleaching (FRAP) experiments in model membranes studying the effect of protein size on the diffusion coefficient [62]. Another model membrane study came to the same conclusion but specifically pointed out that the lipid to protein ratio should be taken into account [18]. A review study suggested that lateral tracer diffusion in a membrane could be divided into two regimes based on the size of the particle: the hydrodynamical Saffman–Delbrück theory for considerably larger inclusions compared to lipids and a free volume theory for particles

with a size equivalent to the lipids, where instead of considering the membrane as a continuum, lipids are assigned in two-dimensional space a non-compressible area based on the space they occupy [63]. Before the end of the nineties, alternative approaches and modifications to the Saffmann–Delbrück theory were done with the help of both experiments and simulations in order to include the lipid to protein ratio into the theory [64, 65].

In 2005, an experimental study showed considerable deviations for the observed diffusion coefficients compared to the Saffman–Delbrück theory, gaining further evidence in 2009, which once again attracted attention into developing the model [66, 67]. It appeared that the diffusion coefficient of a membrane inclusion had a  $1/R$  relation to the inclusion radius similarly to the three-dimensional Stokes–Einstein equation, given by

$$D = \frac{k_B T}{6\pi\mu_f R}, \quad (3.9)$$

rather than a weaker logarithmic dependence as suggested by the Saffman–Delbrück model. A simulation study attempted to solve the issue, and for the smaller particles Saffmann–Delbrück was supported, however, for larger particles even stronger  $1/R^2$  dependence was observed [68]. It was suggested that the failure of Saffmann–Delbrück could be due to local membrane deformation caused by the proteins [69]. Attempts were made in order to move on by omitting Saffman–Delbrück by improving a more complicated numerical but still hydrodynamical model by Hughes et al [70, 71], which was supported particularly for cases with hydrophobic mismatch between the membrane and the inclusion [72]. Later on, another experimental study using giant unilamellar vesicles supported the logarithmic dependence with a linear decrease in diffusion coefficient when moving to crowded conditions, initially claiming that the observed  $1/R$  dependence is a result of sample preparation when using surface-supported bilayers [73]. However, further studies with other proteins showed both  $1/R$  and logarithmic dependencies, which also led to conclusions that the scaling can be affected by protein-dependent membrane deformations [74]. The latest experimental study from 2013 on both vesicles and bilayers strongly supports the Saffman–Delbrück theory [75], but the previous disagreeing results remain unexplained, and simulations from 2017 still show  $1/R$  scaling in crowded conditions [28].

Despite its issues, the simplicity and established status of the Saffman–Delbrück model had made it still appealing for further development. A theoretical derivation

for it, expanding the model for membrane tubes and tethers, was made by Daniels and Turner [40], given by

$$D = \frac{k_B T}{4\pi\mu_m h} \sum_{m=1}^{\infty} \frac{1}{m} \exp\left(-\frac{ma}{r}\right) \cos\left(\frac{ma}{r}\right) \quad (3.10)$$

$$= \frac{k_B T}{4\pi\mu_m h} \left[ \log\left(\frac{r}{a}\right) + O(1) + O(a/r) + \dots \right], \quad (3.11)$$

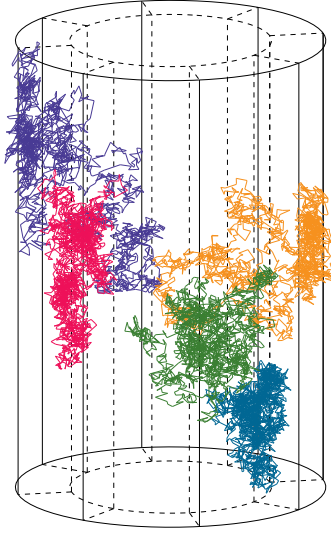
where  $O(x)$  is the big O notation for a growth function, essentially considered as an error term of the model with an  $a/r$  scaling, when the series is cut after the  $O(1)$  term. Though this model made no distinction between the radial and longitudinal directions for the diffusion, something that intuitively could be relevant, it gave grounds for the testing of the Saffman–Delbrück model experimentally, as discussed in section 2.3, and computationally in this thesis.

### 3.4 Displacements on a Cylindrical Surface

Because the displacements of diffusing particles in this thesis occur mainly on the curved surfaces of cylinders, the calculation of these displacements deserves some clarification. For completeness, although the derivation is fairly straightforward, the method for calculating displacements in cylindrical coordinates is demonstrated in this section.

In Figure 3.1, an example of a set of trajectories for transmembrane proteins in the simulated tubular membranes has been shown for illustration and in Figure 3.2 a schematic of a particle displacement on cylinder is drawn for displaying the variables in the displacement calculation. Starting from the point  $\mathbf{x}_1$ , during an ideally infinitesimally small time step, the particle moves to the point  $\mathbf{x}_2$  via the trajectory  $\Delta\mathbf{x}$ , which is the relevant displacement along the surface of the cylinder. Because the displacement occurs on a curved surface, it is not linear. This displacement can be decomposed into components along the tube axis, a straight line denoted with  $\Delta z$ , and around the tube axis, an arc denoted with  $\Delta L$ , which can be calculated by taking the product between the displacement angle  $\theta$  and the tube radius  $r$ , which is considered to be a constant. There is a right angle between these components and together with  $\Delta\mathbf{x}$ , they form a right triangle. With the Pythagorean theorem, the total displacement  $\Delta x$  can also be solved, in addition to the already calculated parallel ( $\Delta z$ ) and perpendicular ( $\Delta L$ ) components.





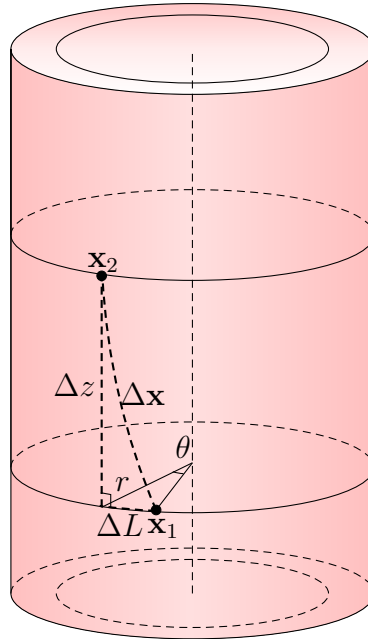
**Figure 3.1** Diffusion trajectories of simulated proteins on a membrane tube demonstrating two-dimensional displacements. Five arbitrarily chosen proteins (each corresponding to a different color) have been allowed to diffuse for  $2 \mu\text{s}$ , and the trajectory of each protein's center of mass has been drawn on a tubular lipid bilayer showcased by a mesh-type representation.

It is noteworthy that the displacement calculation is simple because the radius  $r$  has been set to be constant. If this was not the case, the  $\Delta x$  would still be solvable, but would require more complicated calculation when solving the length of displacement in the radial direction, including either parametrizing the displacement path when  $r$  is changing or solving the length of an arbitrary arc in polar coordinates with the following equation [76]

$$\Delta L = \int_{\theta_1}^{\theta_2} \sqrt{r(\theta)^2 + \left(\frac{dr(\theta)}{d\theta}\right)^2} d\theta, \quad (3.12)$$

where  $\theta_1$  is the angular coordinate in the beginning and  $\theta_2$  in the end of a displacement in the cylindrical coordinate system, and  $r(\theta)$  is described by a line equation if the change in radius would be assumed to be directly proportional to the angular displacement:

$$r(\theta) = \frac{r_2 - r_1}{\theta_2 - \theta_1} \theta + r_1, \quad (3.13)$$



**Figure 3.2** Displacements on a cylindrical surface in polar coordinates.  $\Delta \mathbf{x}$  is the total displacement between points  $\mathbf{x}_1$  and  $\mathbf{x}_2$ ,  $\theta$  is the angular displacement,  $r$  is the radius of the tube,  $\Delta L$  is the displacement arc in angular direction ( $\Delta L = r\theta$ ), and  $\Delta z$  is the displacement along the tube longitudinal axis.

where  $r_1$  is the radius at the beginning and  $r_2$  at the end of a displacement. Special attention would be required when the displacements occur at the angles of  $\theta \approx -\pi \leftrightarrow \pi$ . Solving these derivatives and integrals during each displacement would be computationally heavy for diffusion calculations, where numerous displacements are calculated. In all of the membrane tube simulations, the tube radius changed a maximum of a half a nanometer during the entire simulation, and at shorter time intervals the radius remained insignificant. This makes the approximation for the use of a single value of  $r$  justified. Still, it is arguably more precise to use the mean of tube radii between the beginning and the end of the displacement rather than  $r$ , which is the approach used in this thesis.

## 4 MOLECULAR DYNAMICS SIMULATIONS

To complement experimental tools in various fields, the development of computers and their computing power have revolutionized the way science is done. Computers have been employed to perform calculations, improve algorithms, produce simulations and trajectories, analyze statistics, and much more. Particularly in cell biology, drug development, and materials research, molecular dynamics simulations of varying precision, as well as quantum mechanical calculations, have become an integral part of the state-of-the-art research. Providing an artificial microscope-type of approach with an infinite resolution and possibilities for analysis, simulations can help answer research questions for which experimentalists lack the tools to study. Although simulations still battle the challenges such as the accuracy of the simulation models and for example in the case of atomistic simulations the lack of computing resources for reaching longer time-scales, the encouraging progress in the development of computer hardware and the deeper understanding in simulation methods and parameters give all the reason to suspect that computers have even more importance in research in the future.

In this chapter, the theory of molecular dynamics (MD) simulations, the main research tool of this thesis, will be discussed. Though the principles of performing these simulations are universal, an emphasis will be on the software package GRO-MACS [77], since it has been used to carry out the simulations of this thesis. In addition, we will look into some more simulation tools relevant to this work, such as coarse-grained models. All the information in this chapter is based on reference [78], unless mentioned otherwise.

### 4.1 Structures and Topologies

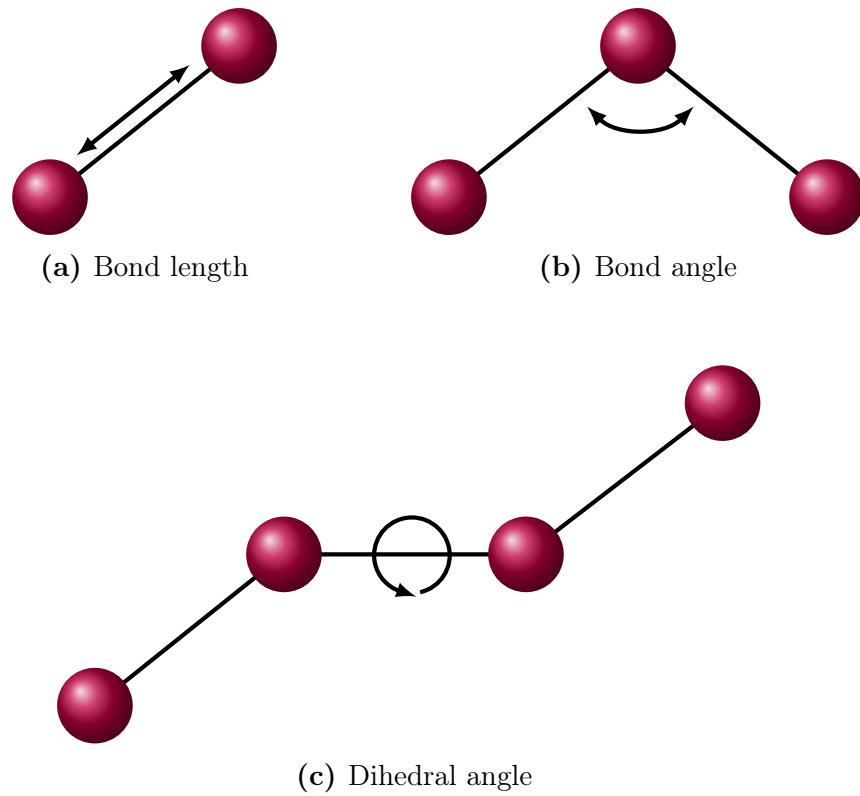
Creating a simulation starts with the preparation of the system to be simulated. When simulating for example proteins on an atomistic scale, the systems used as an input for the simulation can be the result of experimental work trying to resolve

the three-dimensional structure of a protein. Experimental methods aiming for this include nuclear magnetic resonance (NMR), X-ray crystallography, and cryogenic electron microscopy (Cryo-EM). Typically, before starting a simulation, the system requires heavy modifications, and a plethora of tools exist to aid users in setting up their structures for simulations. At first, the system is described essentially by a file containing only the coordinates of each particle (usually atom) of the system, however, they alone are not enough to describe any system fully. Other required properties are listed in the topology of the system, in which each whole molecule is fully characterized.

When it comes to individual atoms of molecules, instead of defining only the element of the atom, the atom type is required. Atoms can behave quite differently depending on the bonds they have with other atoms, and this gives reason to differentiate between atoms of the same element depending on their environment, although the atom types only directly affect the nonbonded forces (discussed later). Also, partial charges of atoms depend on bonded interactions, and if one wishes, the masses of particles can be changed to account for possible atom isotopes.

In the topology description of each molecule, all the particles are assigned an index number to keep track of the particles separately, which makes it easier to define the interconnectivity of the molecule. This includes bonds and angles, which describe arguably the most intuitive bonded interactions. In addition, lists of all four consecutive bonded atoms are made, of which the first three and the last three can be thought to form two separate planes, and the angle between these planes, called the dihedral angle, has relevance in describing how freely a bond can rotate. This is important, for example, when distinguishing between single and double bonds. The bonds, angles, and dihedral angles are illustrated in Figure 4.1. Also, depending on the simulation model, the pairs of particles which are three bonds apart (the last particles of the dihedral angle), so-called 1-4 interaction can be included in the topology if the interaction between such pairs is calculated differently compared to other bonded and nonbonded interactions. This depends on the choice of the force field, which is discussed shortly.

It is worth noting that even though the particle positions and their connections would be properly described, in the beginning, the particles have no velocities. To make the start of the simulation more realistic, the velocities can be generated according



**Figure 4.1** An illustration of bond and angle definitions in a topology. A bond is characterized by its length and stiffness, a bond angle by the angle and its rigidity between three consecutively bonded atoms, and a dihedral angle by the angle between two planes formed by two consecutive bond angles.

to the Maxwell-Boltzmann distribution function:

$$p(\mathbf{v}_i) = \sqrt{\frac{m_i}{2\pi k_B T}} \exp\left(-\frac{m_i |\mathbf{v}|^2}{2k_B T}\right),$$

where  $p$  is the probability of a certain velocity  $\mathbf{v}_i$ ,  $m_i$  is the mass of a particle  $i$ , and  $T$  is the given temperature. The system also has to be confined inside a simulation box before any simulations can be prepared, this will be discussed at the end of this chapter.

## 4.2 Force Fields

A force field consists of a set of equations that are used to calculate the potential energies of the particles in a system, as well as the parameters for each particle and the interactions between them. With the description of the topology, appropriate

parameters are retrieved by the simulation software from the folder describing the force field, many of which are readily bundled with the GROMACS, and to which the user can extend a force field not available on default. The equations for potential energies can be divided into three groups: nonbonded interactions, bonded interactions and restraints, of which some simple yet important examples will be provided. The choice of the force field is one of the most crucial ones when designing a simulation model. Depending on the system and research question, some force fields are particularly designed to reproduce the relevant measurables accurately according to experimental results, while others can lack the relevant parameters altogether, making them completely unsuitable to be used for modeling. Familiarizing oneself with different options for the force field can be daunting but still inevitable for acquiring reliable results from the simulations.

The two most important nonbonded interactions are described by the Lennard-Jones potential  $V_{LJ}$  and the Coulomb potential  $V_c$ . The Lennard-Jones potential is an approximation describing the interactions between two neutral atoms. It contains a repulsive term originating from the Pauli repulsion of the electron orbitals and an attractive term describing van der Waals or dispersion forces when the atoms form temporary electric dipoles. The Lennard-Jones potential is given by

$$V_{LJ}(\mathbf{r}_{ij}) = 4\epsilon_{ij} \left( \left( \frac{\sigma_{ij}}{r_{ij}} \right)^{12} - \left( \frac{\sigma_{ij}}{r_{ij}} \right)^6 \right), \quad (4.1)$$

where  $\epsilon_{ij}$  is the depth of the Lennard-Jones potential well between particles  $i$  and  $j$  and  $\sigma_{ij}$  is the equilibrium distance between the interacting particle pair. These parameters are either pre-calculated based on the atom types of interacting particles with geometric average or Lorentz–Bertholt combination rules or the interactions are listed for all the atom pairs in a matrix of Lennard-Jones parameters from where they are retrieved. Coulomb interaction is the result of two particles with partial electric charges, modeling the average charge distribution of a molecule, which makes the particles either attract or repel each other depending on the signs of the partial charges. The Coulomb interaction is then given by

$$V_c(r_{ij}) = \frac{1}{4\pi\epsilon_0} \frac{q_1 q_2}{\epsilon_r r_{ij}}, \quad (4.2)$$

where  $\epsilon_0$  is the vacuum permittivity constant,  $q_1$  and  $q_2$  are the charges of interacting particles,  $\epsilon_r$  is the permittivity of medium and  $r_{ij}$  is the distance between the atom pair  $ij$ . It is noteworthy that the nonbonded interactions consist of the sum of

both Lennard-Jones and Coulomb potential. Otherwise, for example in the case of charged attracting particles, there would be no repelling potentials between the particles, and they would end up on top of each other, which is both artificial and unsought for.

Bonded potentials can be defined in many ways, and the choice is affected by the force field. Typically, the potentials include simply the already mentioned bonds, bond angles, dihedral angles, but also improper dihedral angles. Other than ordinary dihedral angles, these can be described with the potential of a harmonic oscillator. For bond stretching, the equation is

$$V_b(r_{ij}) = \frac{1}{2}k_{ij}^b(r_{ij} - b_{ij})^2, \quad (4.3)$$

where  $k_{ij}^b$  is a force constant and  $r_{ij} - b_{ij}$  is the difference between the observed bond length and the reference bond length. For bond angle bending, we have

$$V_a(\theta_{ijk}) = \frac{1}{2}k_{ijk}^\theta(\theta_{ijk} - \theta_{ijk}^0)^2, \quad (4.4)$$

where  $k_{ijk}^\theta$  is a force constant,  $\theta_{ijk}$  is the angle between atoms  $i$ ,  $j$  and  $k$ , and  $\theta_{ijk}^0$  is the reference angle between the same atoms. The values of force constants used in these harmonic oscillator models are based on quantum mechanical calculations and experiments so that the bond lengths and angles as well as experimental observables are reproduced in atomistic simulations as well as possible. Improper dihedral angles are used to force some structures into some specific dihedral angle, and therefore, the angle deviation can be thought to have a maximum of 180 degrees, which is similar to angle bending, where the angle can be anything from 0 to 180 degrees. For example, in the case of aromatic rings [79], they need to be forced into planar structures and thus require improper dihedrals. Also, if there is a concern for structure flipping into its mirror image, this can also be prevented with improper dihedrals. The harmonic potential of an improper dihedral angle is described by:

$$V_{id}(\xi_{ijkl}) = \frac{1}{2}k_\xi(\xi_{ijkl} - \xi_{ijkl}^0)^2, \quad (4.5)$$

where  $k_\xi$  is a force constant,  $\xi_{ijkl}$  is the angle between the two planes formed by atoms  $i$ ,  $j$ ,  $k$  and  $l$ , and  $\xi_{ijkl}^0$  is the reference angle between the same planes.

For proper dihedral angles, the potential landscape has to be continuous at and beyond 180 degrees, so it has to be modeled differently. One choice for this is the

following periodic potential  $V_d(\phi_{ijkl})$ :

$$V_d(\phi_{ijkl}) = k_\phi (1 + \cos(n\phi_{ijkl} - \phi_s)), \quad (4.6)$$

where  $k_\phi$  is a force constant,  $n$  is an integer representing angular rotations,  $\phi_{ijkl}$  is the angle between the two planes formed by atoms  $i, j, k$  and  $l$ , and  $\phi_s^0$  is the reference angle between the same planes.

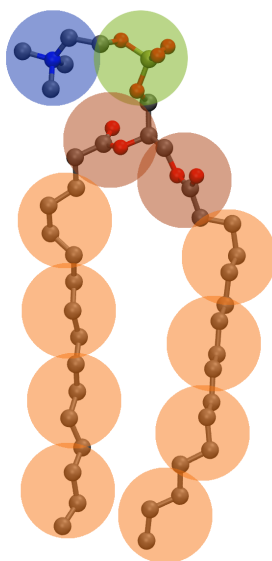
Finally, with restraints, the user can interact with the system in many ways. Dynamics which include restraints are called steered molecular dynamics, and the main difference between such and ordinary dynamics is that although simulations can in principle always be thought to be artificial, steered molecular dynamics contain forces that are not physical, pushing them even further from describing real systems. Still, the user can have a requirement to make a molecule stay in place, within some distance of another object, or intervene in angle or dihedral angle potentials, and all of this can be done with the restraints.

When the bonded interactions, nonbonded interactions, as well as possible restraints are combined with the structure and the topology, the system is ready for the first type of simulation, the energy minimization. However, before moving on, it is important to look into a specific type of force field used in this thesis which, unlike what has been discussed so far, does not contain atoms as its elementary particles.

### 4.3 Martini Coarse-Grained Force Field

One of the main limitations of atomistic molecular dynamics simulations is the reachable simulation time-scales available with current computing resources. For example, activation mechanisms of signaling proteins can take milliseconds, but currently, millisecond-scale simulations, although being the state-of-the-art, can already be quite costly. Also, the proper mixing and equilibration of multicomponent lipid bilayers can be slow and time-consuming, which makes the study of mechanic and dynamic properties of membranes on an atomistic scale expensive. To tackle the time-scale limitations, a concept called Martini was developed to speed up the simulations of biological systems by omitting the atomistic scale of the model by uniting groups atoms into larger sized beads [80, 81, 82, 83]. This drastically reduces the number of computations needed to be performed. The principle idea of the mapping of atoms into beads in Martini force field is demonstrated in Figure 4.2.





**Figure 4.2** A schematic picture elucidating the idea of coarse-graining. In the figure, it has been drawn how atoms of an atomistic scale dipalmitoylphosphatidylcholine (DPPC) lipid have been grouped to spheres representing the beads in a Martini force field. The beads representing the lipid hydrocarbon tails are in orange, glycerol backbone in brown, and the choline head group is modeled by two different bead types in green and blue. In this case, the number of particles is reduced from 130 to 12. In general, approximately 4 heavy atomistic atoms are mapped to a single bead in the Martini model (the hydrogen atoms in the atomistic model have been hidden for clarity).

What kind of consequences does coarse-graining have? First of all, the dynamics of Martini simulations are accelerated by 3–4 orders of magnitude compared to common atomistic models. This is due to the considerable reduction in the degrees of freedom in the system; there are less internal degrees of freedom absorbing energy, and therefore any energy that a molecule receives is more likely to take a form in the translational or rotational energy of the whole molecule, speeding up the system. Another advantage of the Martini model is the significantly smaller number of parameters required to describe the system since essentially the beads in Martini are divided only into four different groups, where they are either polar (hydrophilic), apolar (hydrophobic), nonpolar (miscible in both water and organic solvents), or charged beads. Though each of these groups is further divided into varying levels of interaction strengths, the number of different particle types is still very manageable.

When atomistic models are coarse-grained, one naturally loses the atomistic reso-

lution. This means that for example hydrogen bonds, crucial attracting forces in water solvated systems cannot be modeled accurately. As a result, Martini simulations cannot be used to study, for example, specific protein interactions, which can be highly relevant for the protein's correct function and folding. In fact, excluding loops, Martini fixes the secondary structures with dihedral potential energy functions and it also introduces an artificial elastic network connecting the heavy atoms in the tertiary structures of proteins to keep them from unfolding, which makes it impractical to study conformational changes of proteins with Martini. Another effect of coarse-graining is that modeling water accurately with beads is challenging (4 water molecules are mapped to a single water bead). As an example, it was noticed that water in the Martini model began to freeze at higher temperatures than it was supposed to. To prevent this, the user is advised to replace a fraction of water beads with anti-freeze water particles, which have a higher Lennard-Jones  $\sigma$  parameter, which disturbs the crystallization of ordinary water beads. Also, when protein modeling was made possible in Martini besides lipids, it was found that proteins interacted with each other too strongly, causing almost irreversible protein aggregation [84]. This issue is expected to be resolved in the future releases of the Martini force field. Meanwhile, multiple proteins can be modeled without aggregation by scaling down the protein-protein interactions [85], although this is quite an unsatisfying brute-force approach to correct the force field.

Similarly to atomistic force fields, in Martini the nonbonded interactions are characterized by the Lennard-Jones and Coulomb potentials, although long-range interactions are omitted for better computing performance, and bonds and angles can be described with harmonic potentials. However, the reduction of degrees of freedom also directly decreases the system's entropy, which on the other hand increases the acquired values of free energy. To tackle this, Martini force field compensates the lost entropy with a reduced term for enthalpy so that the acquired free energies and other measurables would match the results of experiments and atomistic models. This sets Martini apart from atomistic force fields, which do not contain such artificial correction [86].

Regardless of all of Martini's drawbacks, it is particularly well suited for studying membrane dynamics, since specific nanoscale interactions are irrelevant and vast amounts of simulation statistics can be produced efficiently and relatively cheaply. When studying protein dynamics, the down-scaling of protein interactions is an appropriate approach, and the simulation results should not be impaired by the

limitations of Martini. This makes it a highly suitable force field for studying transmembrane protein diffusion, and therefore, it has been employed in all of the simulation models of this thesis.

## 4.4 Energy Minimization

After having a well-characterized structure with a topology and a force field, the system is in principle ready for simulations. However, due to possibly quite rough and intrusive building steps of system preparation, most of the particles in the system are most likely very far from equilibrium. The bonds may be too stretched, bond angles unnaturally twisted, or atoms superimposed and starting a simulation from such a state easily leads to an error when the simulation software can tell that the system is strained beyond what can be tolerated.

The relaxation of the system before producing any physical dynamics requires energy minimization. The system has a multidimensional energy landscape with countless energy minima, and it is analytically impossible to find the global energy minimum of the system. The nearest local minima, however, can easily be found. One of the possibilities is to use a *steepest descent* algorithm, where partial derivatives of the potential energies of all particles are calculated, which yields forces. By following the direction of the negative gradient, the direction of the driving force, all the particles can be lead towards the local minimum. By doing this iteratively in small steps for all the particles, the strained structures of the system can be relaxed so that they are ready for simulations based on the laws of physics. The benefits of the steepest descent method include its robustness, simplicity and swiftness, and while the global minimum will most likely not be found with this method, this is completely acceptable for it is not the aim of the energy minimization anyway.

In the steepest descent method, the forces affecting all the particles are calculated first. Then, the new positions are calculated according to the following formula:

$$\mathbf{r}_{n+1} = \mathbf{r}_n + \frac{\mathbf{F}_n}{\max(|\mathbf{F}_n|)} h_n, \quad (4.7)$$

where  $\mathbf{r}_n$  is the initial position of a particle, to which a term is added proportional to  $\mathbf{F}_n$  which is the initial force of a particle, scaled by the maximum force of all particles  $\max(|\mathbf{F}_n|)$  and a term  $h_n$  corresponding to the maximum displacement

allowed during each iteration. The algorithm has finished when either the user-specified number of iterations have been calculated or when the absolute value of the maximum force in the system is lower than a threshold value given as an input.

## 4.5 Equations of Motion

The next step is where an actual molecular dynamics simulation is produced. A trajectory for all the particles in the system is calculated according to the Newton's second law of motion

$$m_i \frac{\partial^2 \mathbf{r}_i}{\partial t^2} = \mathbf{F}_i, \quad i = 1 \dots N, \quad (4.8)$$

where  $m_i$  is the mass of the  $i$ th particle,  $\mathbf{F}_i$  is the total force acting on the particle,  $\mathbf{r}_i$  is the particle's position and  $N$  is the number of all the particles in the system. The forces are calculated as follows:

$$\mathbf{F}_i = -\frac{\partial V}{\partial \mathbf{r}_i}, \quad (4.9)$$

where the potential energy function  $V$  is partially differentiated for all particles in each dimension. These two equations are solved in concession while keeping the pressure and the temperature constant, and the resulting new particle positions are saved. After this, the new energy landscape and the acting forces need to be recalculated for the new positions, resulting in a looping algorithm for calculating a trajectory.

Newton's second law of motion is a second-order differential equation, and analytically solving particle positions via integration is impossible. The integration is done numerically, which requires that time is made discrete by creating time interval called a time step, which is essentially sets the time resolution of a simulation. There are many different algorithms for a numerical integrator to choose from, but the integrator is preferred to be symplectic (conserves the total energy of the system) and time-reversible (integration back and forth in time will result in an identical system). One commonly used group of integrators fulfilling these requirements is the *Verlet* integrators. A modified version of Verlet-integrators is the *leapfrog* algorithm used in this thesis. By using two coupled equations for the position and the velocity of a particle, these two values are calculated alternately with a half a time step difference, and compared to an ordinary Verlet-integrator, only one set of positions and velocities needs to be stored at once. Leapfrog algorithm can be written out as

follows:

$$\mathbf{v}\left(t + \frac{1}{2}\Delta t_{\text{ts}}\right) = \mathbf{v}\left(t - \frac{1}{2}\Delta t_{\text{ts}}\right) + \frac{\Delta t_{\text{ts}}}{m}\mathbf{F}(t) \quad (4.10)$$

$$\mathbf{r}(t + \Delta t_{\text{ts}}) = \mathbf{r}(t) + \Delta t_{\text{ts}}\mathbf{v}\left(t + \frac{1}{2}\Delta t_{\text{ts}}\right), \quad (4.11)$$

where  $\Delta t_{\text{ts}}$  is the duration of the time step. The time step is preferably as long as possible in order to maximize the length of the resulting simulation while minimizing the number of calculations needed to produce it. However, when using a too long time step, the total energy of the system may not be preserved, and the particle displacements between each step may be too great for the simulation to withstand. As a rule of thumb, the time step should be shorter than the shortest-lived phenomenon in the simulation system, which in molecular dynamics simulations is the bond vibrations. Coarse-grained models can reach time steps as large as tens of femtoseconds, but for atomistic simulations, a time step of 1 or 2 femtoseconds is appropriate due to the fast vibrations in the covalent bonds of hydrogen. A bond constraint algorithm like LINCS [87] is usually implemented in order to stabilize bond vibrations enough that the time step of a few femtoseconds does not cause the simulation to crash.

So far, the basic steps of creating a molecular dynamics simulation have been introduced. Figure 4.3 illustrates the workflow for the discussed elements. Next, other relevant parts of running these simulations are discussed.

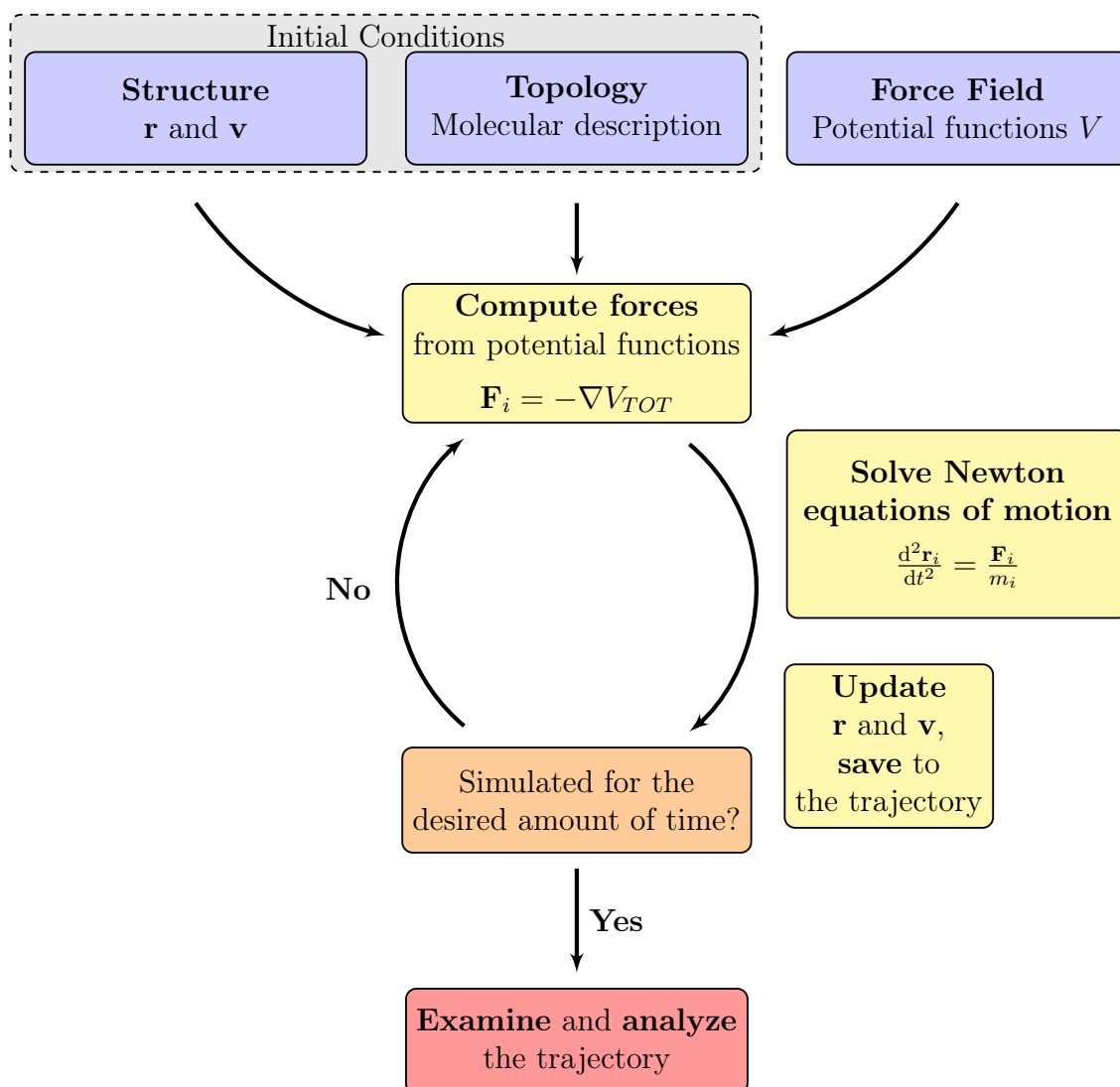
## 4.6 Thermostats and Barostats

As in real experiments, the temperature and the pressure are usually maintained constant in molecular dynamics simulations. This is done with temperature and pressure coupling by using algorithms called thermostats and barostats. Some of the most common ones are discussed here.

Three examples of temperature coupling algorithms are the *Berendsen*, the *stochastic velocity-rescaling*, and the *Nosé-Hoover* thermostats. The Berendsen weak coupling thermostat can be considered to be an external heat bath with a temperature  $T_0$  which drives the system towards the preferred temperature by the following formula:

$$\frac{dT}{dt} = \frac{T_0 - T}{\tau_t}, \quad (4.12)$$

where  $T$  is the temperature of the system and  $\tau_t$  is a time constant with which the



**Figure 4.3** A schematic demonstrating the workflow of molecular dynamics simulation calculation. First, the user needs the structure of the model with particle positions and velocities (which can be generated), and a topology describing the molecules in the system in detail. Parameters for interactions are provided by the force field. In a simulation, the forces acting on particles are calculated by differentiating the potential energy. With an integrator, new positions and velocities are calculated by integrating Newton's equations of motion. After this, if the calculation has been done as many times as the user has specified, the simulation will end and the user can start to work on analyzing the trajectory, otherwise new forces will be calculated to solve the new positions and the loop continues.

coupling time can be adjusted. The Berendsen thermostat can be used with systems far from equilibrium and the strength of temperature coupling is set by the user. It will suppress kinetic fluctuations, failing to result in a correct canonical NVT ensemble, and does not preserve the total energy of the system. However, in the early phases when the system is still equilibrating, Berendsen is a robust choice. An improved version of it is the velocity-rescaling thermostat which introduces an additional stochastic term to enhance the kinetic energy distribution.

After the system is relaxed, a more advanced temperature coupling, the Nosé–Hoover thermostat, is recommended for enabling proper canonical ensemble. Essentially, the Hamiltonian of the system is extended to include terms for a heat bath, similarly to the weak-coupling scheme thermostats like the Berendsen and velocity-rescaling thermostats, but also a friction term proportional to the velocities of the particles. Compared to the Berendsen, which has a strong dampening effect when adjusting the temperature, the Nosé–Hoover has a gentler oscillating approach, and hence it takes far longer for it to bring the temperature to the desired value if initially the system is far from it. The Nosé–Hoover thermostat is discussed in more detail in the reference [88] and in the GROMACS manual.

Barostats in the pressure coupling are the equivalents of thermostats but meant for pressure control. The Berendsen algorithm for pressure is given by:

$$\frac{d\mathbf{P}}{dt} = \frac{\mathbf{P}_0 - \mathbf{P}}{\tau_p}, \quad (4.13)$$

where  $P_0$  is the target pressure matrix,  $P$  is the pressure matrix of the system, and  $\tau_p$  is an adjustable pressure coupling time constant. Unlike when using the Berendsen thermostat, the barostat allows the size of the simulation box (discussed in more detail shortly) change. This is done by something called the *scaling matrix*, which rescales not only the box dimensions but all the coordinates of the particles in the system. For example, in the presence of high pressure, the simulation box will shrink and make the system more compact. In the case of semi-isotropic simulation systems such as lipid bilayers, it is possible and advised to control the pressures separately in the parallel and orthogonal directions with respect to the membrane. As a rule of thumb, the symmetry of the system determines the symmetry of the barostat as well. A semi-isotropic barostat allows the box to simultaneously stretch and squeeze, which can be required for example for the lipids to reach the equilibrium area per lipid.

Similarly to the thermostats, another more sophisticated barostat, the *Parrinello–Rahman* barostat, is meant to be used after the system has moved closer to the equilibrium. In theory, Parrinello–Rahman produces the correct NpT ensemble, which can be difficult to do for the Berendsen barostat especially in the case of small simulations. Similarly to Nosé–Hoover, the Parrinello–Rahman approach introduces extensions to the Hamiltonian of the system, and adjusts the pressure in an oscillating fashion. If used when being too far from the equilibrium pressure, these oscillations can be great enough to make the simulation crash, thus, the Berendsen is a preferable choice for equilibrating. The Parrinello–Rahman algorithm is discussed more in the reference [89] and in the GROMACS manual.

## 4.7 Long-Range Interactions and Periodic Boundary Conditions

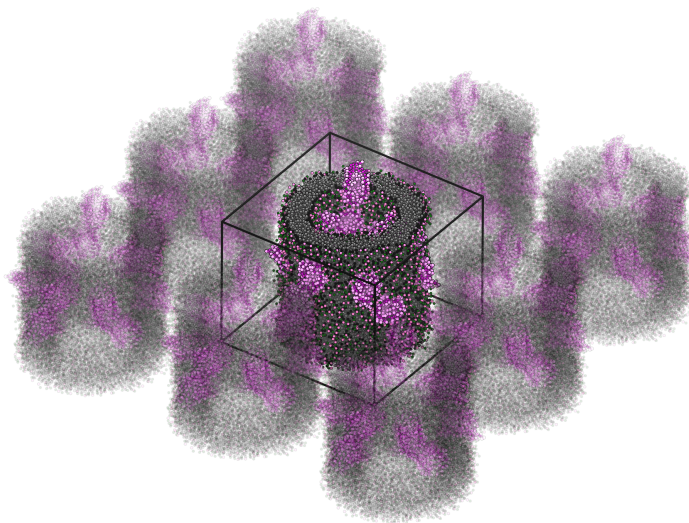
The nonbonded Coulomb and Lennard-Jones interactions comprise the long-range interactions in molecular dynamics simulations. To make their calculation feasible, GROMACS uses a cut-off limit beyond which these interactions are omitted; in the case of the Coulomb potential, this makes sense since it has  $1/r^2$  scaling after all. The interactions at the borders of the simulation box, however, require special attention.

As already discussed, part of the simulation setup is the specification of the restricted area, a simulation box, within which all the particles reside. The shape does not necessarily have to be a cuboid; when simulating proteins solvated in water, rhombic dodecahedron is a much more economical choice for shape since it eliminates the unnecessary water particles at the corners of the system. Still, a cuboid is usually preferred for the simplicity of designing analysis tools for trajectories simulated with this box shape.

To make the simulation model as physical as possible, the borders of the box are treated with periodic boundary conditions (PBC), meaning that on the other side of the box border, there is a perfect translated system replica, with which all of the particles can interact with and which makes the model mimic an infinite system. This is why it is common to call the simulation box as a PBC box. An efficient algorithm for the calculation of electrostatic interactions, the particle mesh Ewald method, is compatible with the PBC, making it a natural choice to treat the system boundaries this way. Figure 4.4 demonstrates the concept of periodic boundary



conditions.



**Figure 4.4** An illustration of periodic boundary conditions in molecular dynamics simulations. In the middle, there is one of the model tube structures studied in this thesis. On the other sides of the faces of the cuboid, there are periodic images of the system, with which the tube structure can interact with. This creates the illusion of an infinite system. Images exist above and below the tube as well, however, they have been left out for clarity.

The PBC are a good representation of a continuous system without artificial edges and is still computationally efficient. Yet, it causes its share of *artifacts*, unphysical errors resulting from the simulation model. Primarily, it is important to ensure that the periodic images preserve the symmetry of the system and that the box size in all dimensions is greater than the cut-off radius of long-range interactions. Otherwise, all the particles would be interacting with their own periodic boundary images. In addition, according to the minimum-image convention, interactions are always calculated only with the closest periodic image. Another noteworthy point is that PBC has been noticed to hinder diffusion rates of molecules proportionally to the PBC box size [90, 91, 92, 93]. This has been argued to be due to the anisotropic scaling of the simulation box. In this thesis, diffusion has been studied by analyzing long simulations where particles are allowed to cross the PBC border multiple times, which makes this artifact crucial to be acknowledged. The artifact is greater the smaller the box is, and fortunately, in this thesis, the simulation boxes for the tubular structures are relatively large. Also, for ordinary bilayer simulations, tools exist for correcting the obtained diffusion coefficients by taking the PBC box dimensions into account [94]. Regardless, when discussing the results of this thesis, the PBC artifacts

must not be ignored.

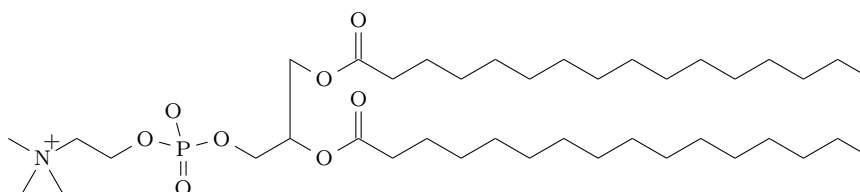
## 5 MODEL AND SIMULATION DETAILS

In this chapter, the practical execution of this study is discussed. First, it is explained how the model membrane structures were prepared. Next, the relevant simulation parameters, such as the physical conditions of the simulation models and the simulation production parameters are given, and finally, the process of data analysis is explored. All the system preparation and simulation was done with the GROMACS version 4.6.7 unless mentioned otherwise.

### 5.1 Building the Tubular Bilayers

The lipid used in the membranes of this thesis is dipalmitoylphosphatidylcholine, or DPPC, which allows direct comparison with earlier simulation results. The structural formula of DPPC is presented Figure 5.1. The protein chosen for the study is a monomeric outer membrane porin G or OmpG [95], available at the Protein Data Bank with code 2F1C [96, 97, 98]. It is found in *Escherichia coli* and it mediates the translation of ions and nutrients across membranes. In this study, the protein parts extending to the solvent have been removed to eliminate hindering effects caused by water. The protein is appropriate for its size, symmetry, and hydrophobic match.

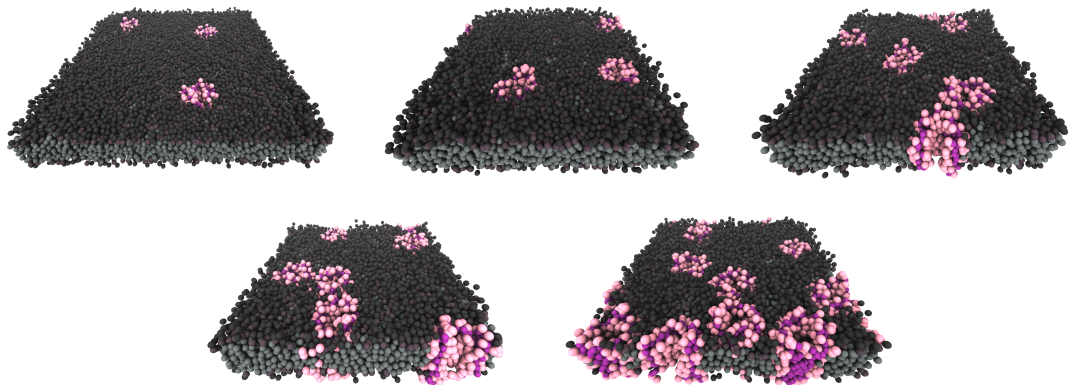
The structures and topologies for Martini coarse-grained lipids, including DPPC, are part of the force field distribution and downloadable from the Martini website. Martini force field version 2.2 was used throughout this study. The modified and



**Figure 5.1** A structural formula of the dipalmitoylphosphatidylcholine lipid. It is a relatively short saturated lipid with two palmitic acids as hydrocarbon chains.

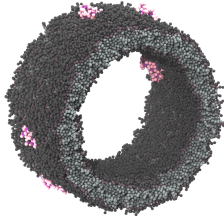
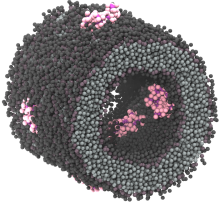

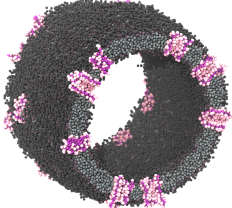
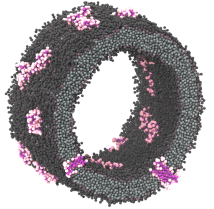
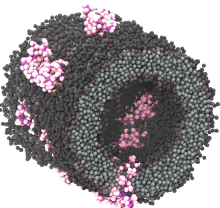
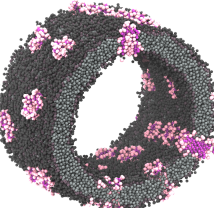
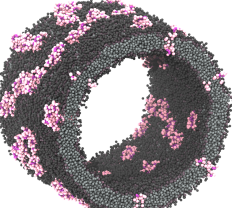
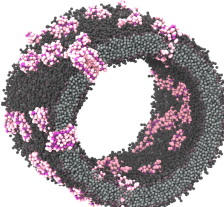
coarse-grained protein structure and topology, used in a previous study [28], were provided by the examiner Matti Javanainen. The protein-protein interactions were reduced to 80 % in order to prevent protein aggregation [84, 85].

With the lipid and protein structures, the tubular structures were built by using PACKMOL software [99]. The PACKMOL runs were not able to converge to proper structures when both lipids and proteins were given as an input, and therefore, lipid tubes and protein tubes were built separately, after which these structures were superimposed. Lipids were present in excess, and all the clashing lipid molecules were removed. Nine tubes were built in total with varying protein concentrations and tube radii. In addition, five planar membranes with varying protein concentrations were built for reference by using membrane structures provided by Javanainen. The planar membranes are shown in Figure 5.2 and tubes in Table 5.1.



**Figure 5.2** Rendered pictures of the planar membranes studied in this thesis. The lipid per leaflet to protein ratios range from dilute (400:1) to concentrated (50:1).

The structure specifics are listed in Table 5.2. In tubular membranes, some lipids were found to be trapped inside the proteins, and thus they were removed from the structure in the early stages of simulations. Therefore, the number of lipids in the tubular systems do not match the exact lipid to protein ratios that the thesis aimed for. Also, the 5- and 10-nanometer tubes equilibrated to structures with slightly larger tube radii than what was designed. However, considering the aim of this thesis to find the relation between diffusion rates, curvature, and protein crowding, these deviations are not significant.

		Tube radius		
		5 nm	10 nm	15 nm
Lipid:Protein ratio	400:1			
	200:1			
	100:1			
	75:1			
	50:1			

**Table 5.1** Rendered pictures of the tubular membranes studied in this thesis. The radius of the tubes varied from approximately 5 nanometers to 15 nanometers, and the lipid to protein ratios from approximately 400:1 to 50:1. The exact values can be found from Table 5.2.

L:P ratio	Average radius (nm)	OmpG	DPPC	Water	Water (antifreeze)	Na <sup>+</sup>	Cl <sup>-</sup>	Box width x/y (nm)	Box height z (nm)
Planar	400:1	3	2400	35733	3970	473	425	27.8	11.0
	200:1	3	1200	19271	2141	266	218	20.2	11.2
	100:1	5	1000	17391	1932	258	178	19.2	11.1
	75:1	6	900	16626	1847	257	161	18.8	11.1
	50:1	9	900	24522	2725	380	236	19.8	13.4
Tubular	200:1	5	1991	35526	3699	473	392	27.1	12.8
	75:1	12	1784	39937	4231	584	392	23.1	16.4
	$\infty$ :1	0	3986	95316	10150	1205	1125	34.6	16.2
	400:1	5	3986	95316	10150	1165	1165	33.4	17.5
	200:1	10	3961	101586	11139	1326	1166	34.0	17.9
	100:1	17	3351	90250	9597	1239	967	33.5	16.5
	75:1	22	3259	103320	11376	1443	1091	35.2	16.7
	50:1	30	2922	94839	10345	1402	922	39.9	15.8
	200:1	15	5984	224600	25120	2879	2639	44.1	21.7
	75:1	35	5184	204382	22842	2791	2231	41.8	22.3

**Table 5.2** The particle numbers, tube radii, and simulation box dimensions of all studied systems. The target tube radii and lipid to protein ratios could not be achieved exactly, but with a reasonable accuracy considering the aim of the thesis.

## 5.2 Simulation Runs and Related Parameters

The tubular and planar membrane structures were thoroughly energy minimized by using the steepest descent algorithm during each system preparation step, which included the solvation, addition of ions to neutralize the charge of the system and the replacement of 10 % of water particles with anti-freeze water particles. The planar membranes were then simulated for 45  $\mu\text{s}$  and the tubular membranes with proteins for 145  $\mu\text{s}$ , both with a leap frog integrator and a time step of 20 fs. The first 100  $\mu\text{s}$  of the tubular membrane simulations were done with isotropic Parrinello–Rahman pressure control of 1 bar and with a time-constant of 50 ps, for this prevented the tubes from collapsing and allowed water to flow through the transmembrane porin proteins in order to equilibrate the water pressures between the inside and the outside of the tube. For the planar membranes and for the rest of the remaining simulation time of tubular membranes, semi-isotropic pressure control was used with the same values of pressure and time-constant. Out of the total simulation time, only the last 30  $\mu\text{s}$  was used for data analysis. The tube without proteins was simulated for 15  $\mu\text{s}$ , of which the first 5  $\mu\text{s}$  was omitted, and because this system was made from the 10-nanometer tube with 400 to 1 lipid to protein ratio by removing the proteins, this was sufficient. The temperatures were controlled with a velocity-rescaling thermostat at a temperature of 315 K to keep the DPPC bilayer fluid, with the temperatures of the membrane and the solution controlled separately, with a time constant of 1 ps. The Coulomb and van der Waals interactions were cut off at 1.1 nm. LINCS algorithm was used to constrain the bead bond lengths between position updates [87].

## 5.3 Analysis Tools

By using GROMACS implemented manipulation tools, the center of mass motion trajectories of all the membrane molecules (lipids and proteins) in each system were produced. This was done in order to export the particle motions to an external program because GROMACS is not able to calculate diffusion coefficients for particles confined to cylindrical surfaces like in this thesis. An analysis script was written with Matlab, and to verify its accuracy, it was also used to calculate the diffusion coefficients in planar membranes, something that GROMACS can do. The result comparison confirmed that the script worked correctly. To simplify further analysis, the PBC treatment was removed with GROMACS before moving on to MATLAB analysis.

		Water height ( $\pm 2\%$ ) (nm)	System lateral size ( $\pm 2\%$ ) (nm)	Membrane viscosity ( $\times \pm 500\%$ ) (poise cm)	Measured diffusion coefficient ( $\pm 30\%$ ) ( $\frac{\text{cm}^2}{\text{s}}$ )
Proteins	400:1	6.8	27.8	$1.2 \times 10^{-8}$	$1.08 \times 10^{-7}$
	200:1	7.0	26.1	$2.0 \times 10^{-8}$	$0.62 \times 10^{-7}$
	100:1	6.8	19.3	$3.0 \times 10^{-8}$	$0.42 \times 10^{-7}$
	75:1	6.8	18.8	$4.0 \times 10^{-8}$	$0.29 \times 10^{-7}$
	50:1	9.1	19.8	$4.0 \times 10^{-8}$	$0.10 \times 10^{-7}$
Lipids	400:1	6.8	27.8	$1.2 \times 10^{-8}$	$6.21 \times 10^{-7}$
	200:1	7.0	26.1	$2.0 \times 10^{-8}$	$5.14 \times 10^{-7}$
	100:1	6.8	19.3	$3.0 \times 10^{-8}$	$3.87 \times 10^{-7}$
	75:1	6.8	18.8	$4.0 \times 10^{-8}$	$3.19 \times 10^{-7}$
	50:1	9.1	19.8	$4.0 \times 10^{-8}$	$1.83 \times 10^{-7}$

**Table 5.3** The parameters used for correcting diffusion coefficients calculated from the MSD curves. In the brackets, relative errors (taken into account during the PBC free diffusion coefficient estimation) and the units for the parameters are given. For proteins, hydrodynamic radius of 2.13 nanometers, based on the effective radius argued in the supplementary information of the reference [28] was used, and for lipids, the value of 0.45 nanometers was used as advised by the method author [94], both with 10 % error. The used values for membrane viscosities were educated estimations, however, the error margins were given to be so large that the input values were irrelevant, and the method succeeded in producing reasonable diffusion coefficient estimates regardless. For all the systems, the water viscosity was set to be  $0.007 \pm 5\%$  poise, interleaflet coupling to  $2.4 \cdot 10^4 \frac{\text{poise}}{\text{cm}}$ , and the number of iterations to 200000. Note that the membrane viscosity, as in the Saffman–Delbrück formula, has been multiplied with the membrane thickness, hence the unit.

The main analysis included the calculation of mean squared displacement graphs for proteins and lipids in all of the systems. In a basic MSD analysis, all the particle displacements are both time and ensemble averaged, meaning that for a single particle the time averaged mean square displacement  $\overline{\delta_i^2(\Delta t)}$  is calculated as follows [27]

$$\overline{\delta_i^2(\Delta t)} = \frac{1}{T_{\text{tot}} - \Delta t} \int_0^{T_{\text{tot}} - \Delta t} (\mathbf{r}_i(t + \Delta t) - \mathbf{r}_i(t))^2 dt,$$

where  $T_{\text{tot}}$  is the total simulation time and  $\Delta t$  is the displacement time. The en-



semble average over these time averages, calculated with

$$\langle \overline{\delta_i^2(\Delta t)} \rangle = \frac{1}{N} \sum_{i=1}^N \overline{\delta_i^2(\Delta t)},$$

is the MSD used for the diffusion analysis. To the acquired MSD graphs, the equations (3.5) and (3.7) were fitted in order to solve the diffusion coefficients and the anomalous diffusion exponents. Also, when appropriate, the Saffman–Delbrück formula extension was fitted to the obtained data. The time-dependent diffusion exponents were calculated by making a linear fit on the logarithm data of the mean squared displacement and by extracting the slope. The simulated diffusion coefficient values for planar membranes were fixed according to the bayesian approach explained in the reference [94] with the parameters listed in Table 5.3. Finally, the hydrodynamic properties of water were studied with GROMACS tools, to explore the confining effects of the membrane, and to discuss whether it might have an impact on the lateral diffusion coefficients in the tubes. All of the figures representing molecular dynamics structures in this thesis have been rendered by using VMD (Visual Molecular Dynamics) software [100].

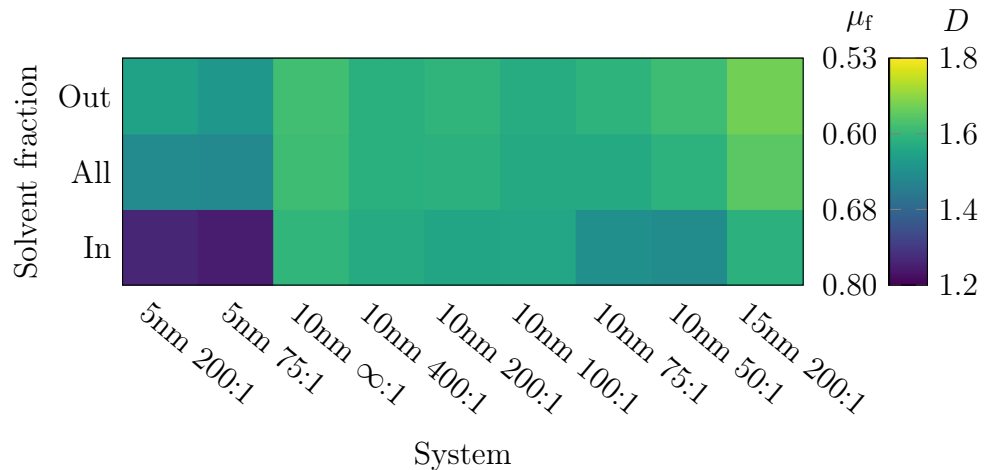
## 6 RESULTS AND DISCUSSION

In this chapter, the analysis results of the coarse-grained simulations are discussed. This includes the acquired diffusion coefficients of both proteins and lipids, decomposed into the radial and longitudinal directions in the case of tubular membranes, as well as anomalous diffusion exponents. The results for diffusion coefficients are finally presented as a function of membrane curvature, answering the original research question of how the curvature affects the mobility of embedded membrane proteins.

### 6.1 The Viscosity of Water

Before jumping into the lipid and protein diffusion results, it is interesting to discuss the viscosity of water in the systems with tubular membrane shapes. According to the Saffman–Delbrück formula ( 3.8), an increase in the viscosity of the surrounding fluid decreases the Saffman–Delbrück length, resulting in lower diffusion coefficients predicted by the theory. In membrane tubes, the mobility of water is confined by the membrane itself, and this should be reflected on the water viscosity according to the Stokes–Einstein equation ( 3.9). This is obvious in the perpendicular directions to the tube longitudinal axis, but the effect should be present to some degree even in the longitudinal direction due to the drag caused by the membrane surface (similarly to the no-slip condition for the flow of liquid at the liquid-solid interface used in the modeling of fluid dynamics).

In Figure 6.1, a heatmap comparing the diffusivities of water in the longitudinal direction in the tubular membranes is presented. In the case of smaller tubes with a tube radius around 5 nanometers, the water inside the tube experiences a noticeable decrease in the diffusion coefficient, which can be interpreted as an increase in the viscosity. If the Saffman–Delbrück theory is to be applied for membrane tubes that confine the solvent to this extent, it is worth to consider whether the used value for solvent viscosity has relevance for the results. Luckily, tubes with such a small



**Figure 6.1** Density plot of the diffusion coefficients and viscosities of solvent along the longitudinal axis, also separately for water inside and outside of the tube. Units of diffusion coefficient  $D$  are in  $10^{-5} \frac{\text{cm}^2}{\text{s}}$  and dynamic viscosity  $\mu_f$  in  $\text{mPa} \cdot \text{s}$  (0.01 poise). The viscosities have been calculated by using the Stokes–Einstein equation (formula 3.9), where as the radius of the particle  $r$  the Lennard-Jones equilibrium distance  $r = 2^{\frac{1}{6}} \cdot \sigma \approx 0.48 \text{ nm}$  has been used, where  $\sigma = 0.43 \text{ nm}$ , a parameter of the Martini force field. For reference, Martini water has been measured to have a dynamic viscosity of  $0.7 \text{ mPa} \cdot \text{s}$ , close to the experimental result of  $0.55 \text{ mPa} \cdot \text{s}$  [101].

radius are not prevalent, and therefore, in general, the changes in water viscosity can be assumed to be negligible.

## 6.2 Diffusion Coefficients and Exponents

The main results of this thesis — the lateral and decomposed diffusion coefficients and diffusion exponents of proteins and lipids in tubular and planar membranes — are presented next. All the diffusion coefficients have been obtained by fitting the formula (3.5) to the mean squared displacement data, which is both time and ensemble averaged. The MSD data is presented in the appendix A, with the fitting starting from the displacements time of 100 nanoseconds and ending at 2000 nanoseconds. The values for the diffusion exponents have been acquired by fitting the formula (3.7) to the same data, and from which only the exponent has been extracted. In addition, the graphs for the time evolution of the diffusion exponents are given in the appendix A. When applicable, the GROMACS software package tools for calculating the diffusion coefficients have been used to ensure and prove the correctness of the MSD calculation and the diffusion analysis tools used for

	Planar	Planar corrected (95 % CI)	GROMACS	
Proteins	400:1	$0.93 \pm 0.03$	2.48 (2.11–2.83)	$1.08 \pm 0.10$
	200:1	$0.61 \pm 0.03$	1.68 (1.43–1.92)	$0.62 \pm 0.18$
	100:1	$0.39 \pm 0.05$	1.50 (1.29–1.72)	$0.42 \pm 0.11$
	75:1	$0.24 \pm 0.01$	1.16 (0.98–1.33)	$0.29 \pm 0.05$
	50:1	$0.10 \pm 0.01$	0.47 (0.25–0.65)	$0.10 \pm 0.03$
Lipids	400:1	$6.19 \pm 0.01$	8.39 (7.24–9.48)	$6.21 \pm 0.01$
	200:1	$5.15 \pm 0.02$	7.29 (6.24–8.23)	$5.13 \pm 0.07$
	100:1	$3.90 \pm 0.01$	6.19 (5.35–7.02)	$3.87 \pm 0.03$
	75:1	$3.14 \pm 0.03$	5.34 (4.58–6.06)	$3.19 \pm 0.03$
	50:1	$1.86 \pm 0.07$	3.23 (1.69–4.56)	$1.83 \pm 0.24$

**Table 6.1** The protein and lipid diffusion coefficients in planar membranes, units in  $10^{-8} \frac{\text{cm}^2}{\text{s}}$  for proteins and  $10^{-7} \frac{\text{cm}^2}{\text{s}}$  for lipids. In the Planar column, the slopes of the MSD curves have been divided with 4 according to the formula of the MSD of a Brownian particle in two-dimensional space. In the Planar corrected column, the results of Planar column have been extrapolated for correcting the PBC artifacts. In the GROMACS column, the uncorrected diffusion coefficient from lateral MSD has been calculated with GROMACS package for comparison.

	5 nm	10 nm	15 nm	
Proteins	400:1	$1.52 \pm 0.05$		
	200:1	$1.13 \pm 0.01$	$1.17 \pm 0.02$	$1.50 \pm 0.03$
	100:1		$0.97 \pm 0.01$	
	75:1	$0.39 \pm 0.03$	$0.60 \pm 0.01$	$0.61 \pm 0.05$
	50:1		$0.45 \pm 0.00$	
Lipids	$\infty:1$		$7.31 \pm 0.07$	
	400:1		$6.59 \pm 0.01$	
	200:1	$5.56 \pm 0.04$	$5.87 \pm 0.03$	$6.00 \pm 0.05$
	100:1		$4.51 \pm 0.02$	
	75:1	$3.24 \pm 0.04$	$3.45 \pm 0.04$	$3.54 \pm 0.06$
50:1		$2.28 \pm 0.03$		

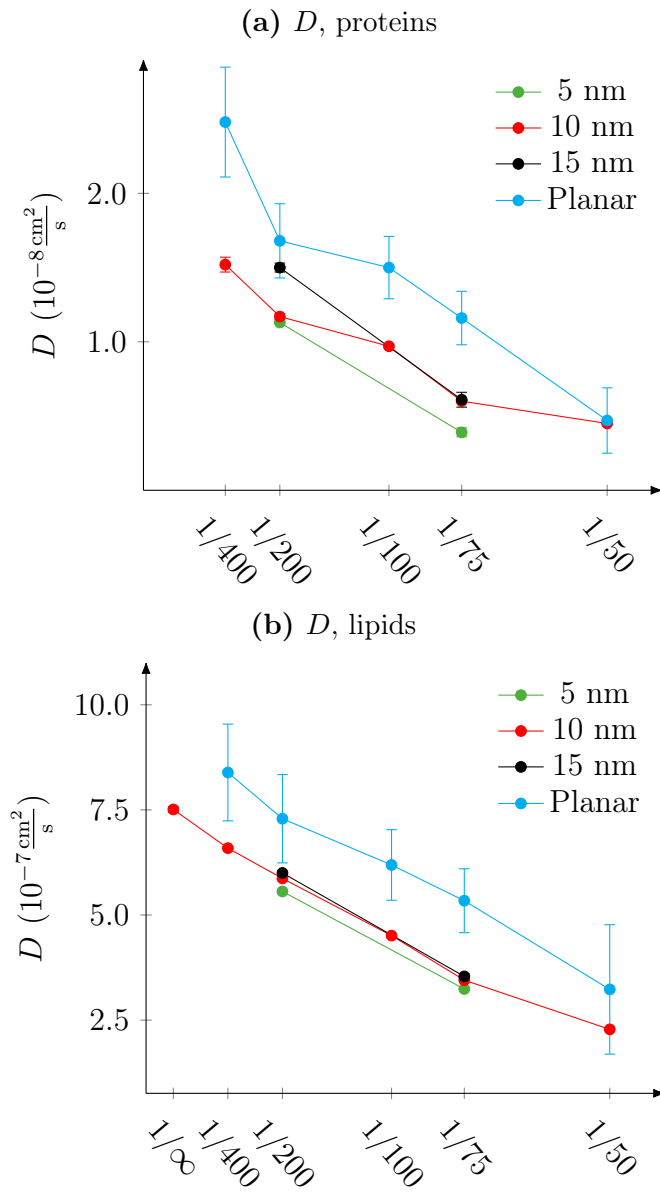
**Table 6.2** The protein and lipid diffusion coefficients in tubular membranes, units in  $10^{-8} \frac{\text{cm}^2}{\text{s}}$  for proteins and  $10^{-7} \frac{\text{cm}^2}{\text{s}}$  for lipids. The slopes of the MSD curves have been divided with 4 according to the formula of the MSD of a Brownian particle in a two-dimensional space.

	5 nm	10 nm	15 nm	Planar		
Proteins	400:1		$1.02 \pm 0.03$	$0.92 \pm 0.03$		
	200:1	$1.00 \pm 0.03$	$0.95 \pm 0.02$	$1.02 \pm 0.01$	$0.90 \pm 0.02$	
	100:1		$0.98 \pm 0.01$		$0.87 \pm 0.08$	
	75:1	$0.87 \pm 0.01$	$0.89 \pm 0.03$	$0.87 \pm 0.02$	$0.87 \pm 0.02$	
	50:1		$0.93 \pm 0.02$		$0.71 \pm 0.05$	
	400:1 z		$1.05 \pm 0.04$		—	
	200:1 z	$1.02 \pm 0.01$	$0.97 \pm 0.04$	$1.05 \pm 0.02$	—	
	100:1 z		$1.01 \pm 0.01$		—	
	75:1 z	$0.90 \pm 0.04$	$0.90 \pm 0.05$	$0.88 \pm 0.05$	—	
	50:1 z		$0.94 \pm 0.02$		—	
	400:1 $\theta$		$0.92 \pm 0.02$		—	
	200:1 $\theta$	$0.88 \pm 0.03$	$0.87 \pm 0.02$	$0.96 \pm 0.02$	—	
	100:1 $\theta$		$0.86 \pm 0.02$		—	
	75:1 $\theta$	$0.71 \pm 0.02$	$0.85 \pm 0.01$	$0.81 \pm 0.00$	—	
	50:1 $\theta$		$0.84 \pm 0.05$		—	
	Lipids	$\infty$ :1		$1.00 \pm 0.01$		
		400:1		$1.00 \pm 0.00$		$1.00 \pm 0.00$
		200:1	$0.98 \pm 0.00$	$0.99 \pm 0.00$	$1.00 \pm 0.01$	$0.99 \pm 0.00$
100:1			$0.99 \pm 0.00$		$0.98 \pm 0.01$	
75:1		$0.95 \pm 0.00$	$0.95 \pm 0.01$	$0.95 \pm 0.00$	$0.96 \pm 0.01$	
50:1			$0.92 \pm 0.02$		$0.88 \pm 0.01$	
$\infty$ :1 z			$1.00 \pm 0.02$		—	
400:1 z			$1.01 \pm 0.00$		—	
200:1 z		$0.99 \pm 0.00$	$0.95 \pm 0.01$	$1.01 \pm 0.01$	—	
100:1 z			$1.01 \pm 0.01$		—	
75:1 z		$0.97 \pm 0.01$	$0.95 \pm 0.02$	$0.96 \pm 0.00$	—	
50:1 z			$0.95 \pm 0.02$		—	
$\infty$ :1 $\theta$			$1.00 \pm 0.00$		—	
400:1 $\theta$			$0.99 \pm 0.00$		—	
200:1 $\theta$		$0.97 \pm 0.00$	$0.99 \pm 0.00$	$0.99 \pm 0.00$	—	
100:1 $\theta$			$0.97 \pm 0.01$		—	
75:1 $\theta$		$0.93 \pm 0.01$	$0.94 \pm 0.01$	$0.94 \pm 0.01$	—	
50:1 $\theta$			$0.86 \pm 0.02$		—	

**Table 6.3** The protein and lipid diffusion exponents, also separately for longitudinal and radial directions. The values have been acquired by extracting the diffusion exponent when the formula 3.7 has been fitted to the MSD data. The time evolution of the diffusion exponents can be seen in the plots in the appendix A.

the tubular membranes. The GROMACS results are not used for other purposes. Particularly in the cases where the MSD curves are not ideally linear, the small deviations between some of the results given by the GROMACS and the tubular membrane diffusion analysis tool for diffusion coefficients are explained by the fact that in the linear regression, GROMACS implements higher weights for short displacement times since there is more data available for that region of the MSD curve. The choice of fitting method is a matter of taste, and both of these approaches have their slight advantages and disadvantages, with no significant impact on the analysis. For planar membranes, the PBC corrected diffusion coefficients are also presented. The diffusion coefficients in planar membranes are given in Table 6.1, the lateral diffusion coefficients in tubular membranes in Table 6.2, the decomposed diffusion coefficients for tubular membranes in Table 6.4, and all the diffusion exponents in Table 6.3. In Figures 6.2 and 6.3, the obtained diffusion coefficients have been plotted as a function curvature and in figures 6.5 and 6.4 as a function of membrane curvature. All the error bars in tables and Figures are 95 % confidence intervals, and since only one replica of each system has been studied, the statistical errors are in many cases too small to be visible in the plots.

In the planar systems, the hindering effects on diffusion caused by crowding are similar to what was found in previous simulations [28], even though the used protein composition was heterogeneous in those systems. With a gradual decrease in diffusion coefficient as the system becomes crowded, the mobility of lipids is reduced to almost one-third and for proteins to almost one-fifth of the dilute system diffusion (when focusing on the PBC corrected coefficients). The comparison of the precise values between the studies is not fruitful, even though the same protein, lipid bilayer composition, and coarse-grained force field were used. This is not so much because of the protein heterogeneity in the previous study, but due to the difference in the size of the simulation box. For example, the uncorrected diffusion coefficient in a dilute system was previously found to be approximately  $2 \cdot 10^{-7} \text{cm}^2/\text{s}$ , while in this study, as shown by the Table 6.1, the value is  $0.93 \cdot 10^{-7} \text{cm}^2/\text{s}$ , but because the length of the side of the simulation box in the lateral direction was in the earlier study 61 nanometers, while being 27.8 nanometers in the system of this thesis, obvious PBC artifacts are present. Though the same values for the diffusion coefficients are unachievable, the physics of membrane crowding effects are reproduced. This applies also for the diffusion exponents, where a 0.21 (-23 %) decrease is observed for proteins in planar systems and  $0.1 \pm 0.05$  (from 8 to 14 %) for both lipids and proteins in all tubular systems. However, since the exponents are extracted from



**Figure 6.2** The two-dimensional diffusion coefficients of proteins and lipids in systems of varying radii as a function of lipid per leaflet to protein ratio. The data for planar membranes has been PBC corrected. The established hindering effect on diffusion in crowded planar membranes is reproduced in curved membranes.

the same MSD data without PBC correction, the direct comparison of the values should be avoided.

When it comes to the lateral diffusion of proteins and lipids in tubular membranes, the effects of curvature on diffusion become evident. Though the effects on lipids are expectedly more subtle, the protein diffusion in a system with the 75:1 lipid to protein ratio and 15 nanometer radius of curvature is over 50 % faster compared to 5-nanometer tube, and for a system with the 200:1 lipid to protein ratio, the difference is also over 30 %, as shown by Table 6.2 and Figure 6.2. If compared to planar membranes, the difference would be even greater, but since the planar systems are PBC corrected unlike the tubular systems, this comparison should not be done for the total lateral diffusion. When decomposed into longitudinal and radial components, the longitudinal diffusion can be seen to be consistently faster for both lipids and proteins in all systems compared to the radial diffusion. Although it has not been extensively tested on tubular membranes, it can be assumed that PBC effects are not as considerable in the radial direction of the diffusion compared to the longitudinal, since the absolute displacements remain short in the radial direction (even though it has been shown that PBC affects even the rotational diffusion [93]). If a comparison between the PBC corrected planar diffusion and the uncorrected radial diffusion in tubes for proteins is just, the diffusion along the direction of curvature is shown to be considerably slower; the radial diffusion of proteins in a 5-nanometer tube is slowed to one-fifth in the case of 200:1 lipid to protein ratio system and to almost one-tenth in 75:1 system compared to planar membranes, illustrated in Figure 6.2. This means that the slowdown in diffusion caused by nanoscale curvature is comparable to the effects caused by protein crowding.

### 6.3 Longitudinal and Radial Diffusion

When examining the effect of curvature on the longitudinal diffusion, presented in Figure 6.4, no obvious dependence can be seen. The 5-nanometer system with 75:1 lipid to protein ratio seems to experience relatively strong hindering in the diffusion, which may be due to the environment being both crowded and curved simultaneously. In general though, it seems that the diffusion in radial direction is primarily affected. By intuition, this is sensible since one may assume that the membrane properties in the longitudinal direction should not necessarily depend on the curvature in the radial direction. However, this is in striking contrast to earlier experimental studies by the research group of Prof. Bassereau, discussed in

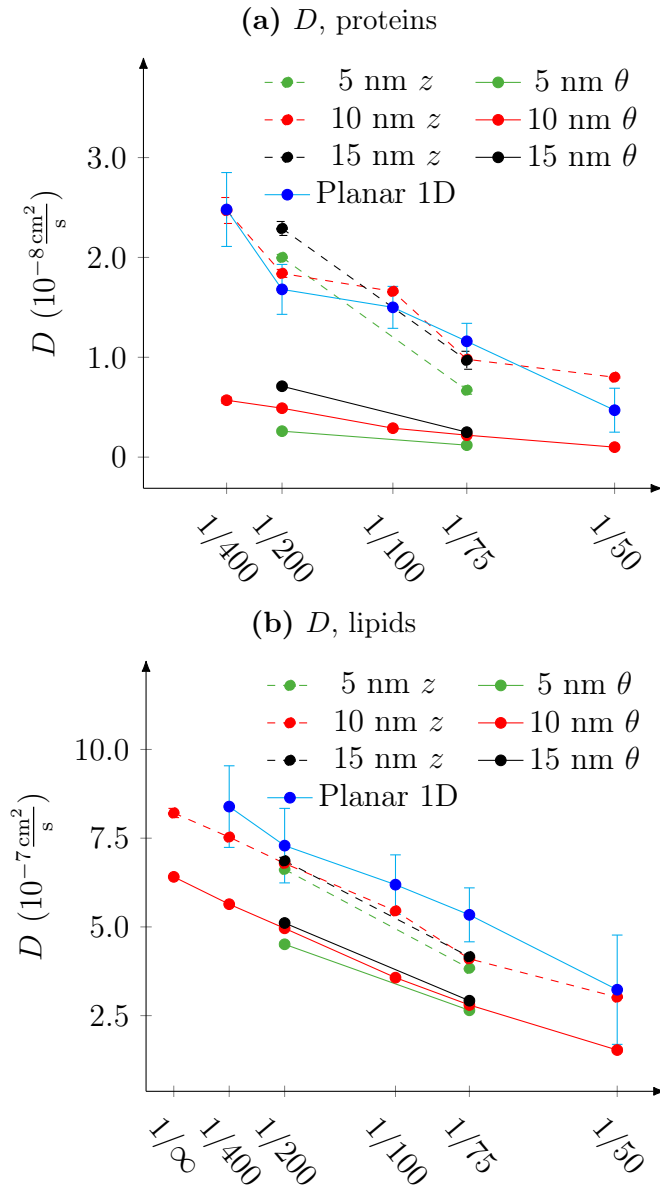


	5 nm	10 nm	15 nm	
Proteins	400:1 z	2.47 ± 0.13		
	200:1 z	2.00 ± 0.03	1.84 ± 0.04	2.29 ± 0.07
	100:1 z	1.66 ± 0.02		
	75:1 z	0.67 ± 0.04	0.98 ± 0.02	0.97 ± 0.09
	50:1 z	0.80 ± 0.00		
	400:1 $\theta$	0.57 ± 0.03		
	200:1 $\theta$	0.26 ± 0.02	0.49 ± 0.02	0.71 ± 0.02
	100:1 $\theta$	0.29 ± 0.01		
	75:1 $\theta$	0.12 ± 0.02	0.22 ± 0.01	0.25 ± 0.02
	50:1 $\theta$	0.10 ± 0.02		
GROMACS	400:1 z	2.48 ± 0.31		
	200:1 z	1.72 ± 0.18	2.24 ± 0.14	2.14 ± 0.14
	100:1 z	1.47 ± 0.15		
	75:1 z	0.68 ± 0.08	1.01 ± 0.03	1.03 ± 0.23
	50:1 z	0.78 ± 0.08		
Lipids	$\infty$ :1 z	8.21 ± 0.13		
	400:1 z	7.53 ± 0.02		
	200:1 z	6.62 ± 0.02	6.79 ± 0.04	6.86 ± 0.10
	100:1 z	5.45 ± 0.05		
	75:1 z	3.83 ± 0.04	4.10 ± 0.03	4.16 ± 0.07
	50:1 z	3.02 ± 0.01		
	$\infty$ :1 $\theta$	6.41 ± 0.02		
	400:1 $\theta$	5.64 ± 0.02		
	200:1 $\theta$	4.51 ± 0.06	4.96 ± 0.02	5.11 ± 0.00
	100:1 $\theta$	3.57 ± 0.01		
75:1 $\theta$	2.65 ± 0.05	2.80 ± 0.04	2.92 ± 0.05	
50:1 $\theta$	1.53 ± 0.06			
GROMACS	$\infty$ :1 z	8.22 ± 0.33		
	400:1 z	7.49 ± 0.09		
	200:1 z	6.42 ± 0.03	6.89 ± 0.03	6.78 ± 0.03
	100:1 z	5.18 ± 0.02		
	75:1 z	3.84 ± 0.08	4.16 ± 0.07	4.21 ± 0.19
50:1 z	3.00 ± 0.08			

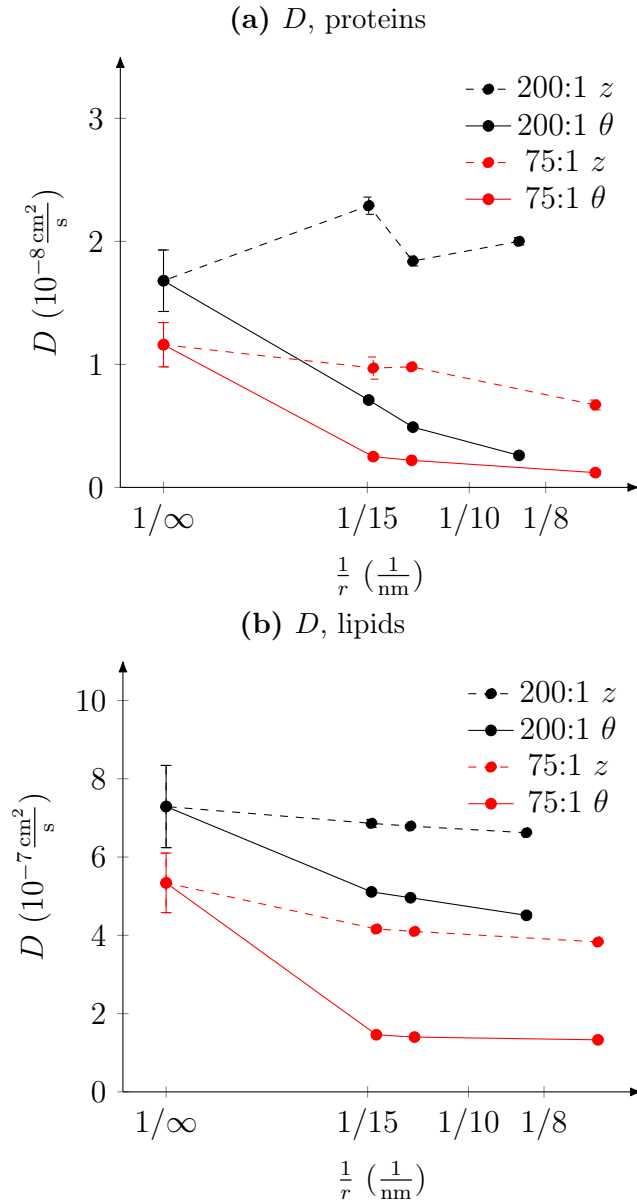
**Table 6.4** The protein and lipid diffusion coefficients in tubular systems, separated into radial ( $\theta$ ) and longitudinal ( $z$ ) dimensions, units in  $10^{-8} \frac{\text{cm}^2}{\text{s}}$  for proteins and  $10^{-7} \frac{\text{cm}^2}{\text{s}}$  for lipids. The slopes of the MSD curves have been divided with 2, according to the formula of the MSD of a Brownian particle in one-dimensional space. Since GROMACS can calculate diffusion in the longitudinal dimension, these results have been included for both lipids and proteins for comparison and result verification.

section 2.3, where the longitudinal diffusion for both proteins and lipids — even in the absence of proteins — was observed to be several times slower in highly curved membranes compared to planar membranes. The disagreement between the simulations and experiments is beyond something that could be explained by the PBC artifacts in the simulations. As a matter of fact, if the longitudinal diffusion in the tubular membrane simulations could be corrected, this would only increase the acquired diffusion coefficients in curved membranes, opposite to what it would require to make the results between the simulations and experiments match.

To understand this, it has to be established that because the results are so profoundly conflicting, either the results by the simulations or the experiments are incorrect, or there is some other aspect that has been neglected completely, inducing contrasting curvature mediated effects in different experiments. Considering the simulations, in addition to problems caused by the PBC, it is fair to question if the systems are properly equilibrated and whether the presented simulations provide sufficient data for reliable diffusion analysis. With a semi-isotropic barostat, long simulation time, and porin proteins allowing water pressure to equalize between the inside and the outside of the tube, the tubes should be properly equilibrated. In order to observe any instability, the tube radius and shape were monitored throughout the simulation, but no considerable changes were seen, indicating that the systems were equilibrated to an extent that they were not driven to change form in any way. When it comes to the acquired data in general, the MSD plots in the appendix A show close to linear curves for all the systems, implying that there should be enough data for accurate fitting. In addition, the alpha exponents in Table 6.3 indicate that the MSD curves are not far from linear. It is worth mentioning though, that for proteins the data is not nearly as ideal as for lipids due to the low number of proteins, leading to less statistics and poorer curve fitting. Naturally, the anomalous diffusion also makes the fitting of the Brownian diffusion model to the data challenging. For example, when Figure 7.6 in the appendix A is examined closely, the slope of the MSD curve for the longitudinal diffusion of proteins in a system with 10-nanometer radius and 200:1 lipid to protein ratio is greater at shorter displacement times of a few hundred nanoseconds compared to longer times, This causes problems in curve fitting and a noticeable difference can be seen in the acquired diffusion coefficient values calculated by the GROMACS and by the written analysis tools for tubular membranes, displayed in Table 6.4. One may also question, whether there is some other issue in the system causing the outlying diffusion coefficient, but since the acquired lipid diffusion coefficient is in line with the other results, this is unlikely.



**Figure 6.3** The one-dimensional diffusion coefficients in longitudinal and radial directions of proteins and lipids in systems of varying radii as a function of lipid to protein ratio. The planar data has been PBC corrected. Regardless of crowding, the difference in longitudinal and radial diffusion is persistent.



**Figure 6.4** One-dimensional diffusion coefficients of proteins and lipids separately in longitudinal and radial directions in systems of varying crowdedness as a function of the inverse of radius. The diffusion is affected in the radial direction strongly by membrane curvature, but no similar effect can be observed for the longitudinal direction.

Nevertheless, these simulation related issues do not seem to be enough to explain the opposing results compared to experiments.

Meanwhile, the authors of the experiments have addressed several factors that might have affected data. The three possibly most relevant of these are the control of tube

radius with membrane tension, the inability to differentiate longitudinal and radial diffusion, and the use of large labeled tracers for tracking. Although in the supplementary information of the reference [41] it was declared that membrane tension should not affect lateral diffusion, this might require a more thorough both experimental and computational study. Monitoring radial diffusion in thin membrane tubes is dauntingly challenging, but if ever possible, results of such experiments would clearly indicate the curvature mediated effects, since the difference between longitudinal and radial diffusion could be studied simultaneously and a reliable comparison could be made. Also, the use of large tracer particles in SPT experiments has been shown to at least reduce the correlation between the diffusing membrane protein and the attached tracer particle within microsecond time scales [102], an issue that may be even more severe on curved surfaces.

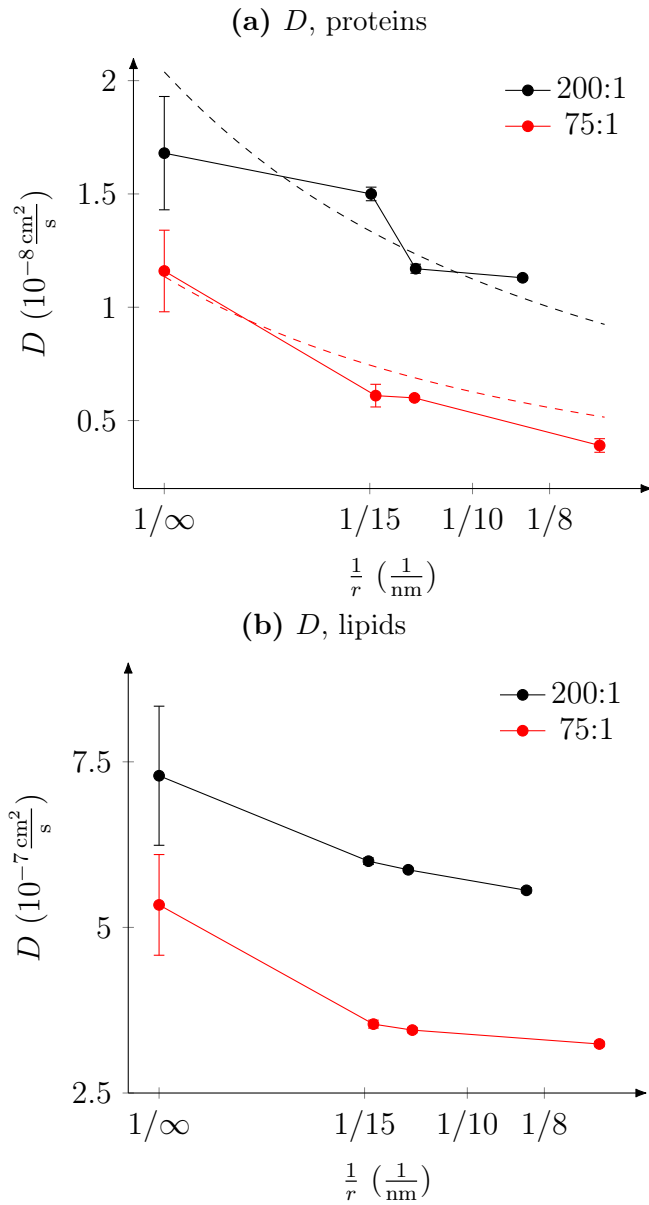
If the results of both the simulations and experiments would be assumed to be correct, there has to be some other key factor affecting the lateral diffusion of proteins in curved membranes. The obvious differences between the simulations and experiments are the proteins and lipids used in the experiments; while the protein used in this work was a modified aquaporin, staying in an upright position in the membrane, the protein in the experimental work by the group of Prof. Bassereau was a slightly smaller voltage-gated potassium channel, which according to the Protein Data Bank prefers a tilted orientation in the membrane. Also, the simulations were set to have 315 K temperature in order to keep the saturated DPPC lipid membrane fluid, while the experiments were done in room temperature by using a mixture of unsaturated lipids. As discussed in section 3.3, it has been heavily speculated that the protein shape and membrane mismatch can in the planar membranes determine, whether the diffusion of proteins has a scaling according to the Saffman–Delbrück theory or the Stokes–Einstein equation. Similar effects could be present in curved membranes as well. To test the possible importance of protein shape, simulations could be done by using, for instance, conical proteins, and a comparison of the results could be made with the cylindrical proteins used in this work. According to Prof. Bassereau, the PI of the reference [41], it was discussed (on 10th of June 2019) that it is plausible that curvature facilitated protein-protein interactions cause the hindering in diffusion, and the strength of the effect or the absence of it is dependent on the shape or the type of the protein. However, the experiments observed the slower longitudinal lipid diffusion in curved membranes containing no proteins. In this work, DPPC lipid with saturated fatty acid chains was used, but in the experiments, a mixture of unsaturated phosphatidic acid and phosphatidylcholine with

tracer labels was used. Therefore, both experiments and simulations with varying lipid compositions could be prepared to further investigate the effect of lipid type on the longitudinal diffusion in curved membranes.

## 6.4 The Extension to the Saffman–Delbrück

Anyhow, the ability of the theory by Daniels and Turner to match transmembrane protein diffusion and membrane curvature was also tested in this work. The theory does not differentiate the diffusion between the longitudinal and radial directions, and therefore the formula ( 3.10) (with the index  $m$  ranging from 1 to 10) has been fitted to the total diffusion data of proteins in Figure 6.5. This is arguably problematic since the diffusion in tubular systems has not been PBC corrected in the longitudinal direction, and therefore, caution is required when interpreting the data. Still, the fit described by the equation matches the data surprisingly well. The dynamic membrane viscosities, the free parameters acquired from the fits are reasonable 0.10 Pas for the system with 200:1 lipid to protein ratio and 0.18 Pas for 75:1, which are in good correspondence with earlier results for membrane viscosities in lipid bilayers in Martini models, considering that membrane crowding increases the membrane viscosity (for example,  $\eta_{\text{eff}}/h \approx 4.73 \cdot 10^{-11} \text{ Pas} \cdot \text{m}/(5 \cdot 10^{-9} \text{ nm}) \approx 0.01 \text{ Pas}$  and  $\eta_{\text{eff}}/h \approx 5 \cdot 10^{-10} \text{ Pas} \cdot \text{m}/(5 \cdot 10^{-9} \text{ nm}) \approx 0.1 \text{ Pas}$ , where the effective dynamic membrane viscosity  $\eta_{\text{eff}}$  has been divided by an approximate membrane thickness to make the values comparable to the membrane viscosities used in this thesis [103, 104]). Thus, with reservations due to the PBC artifacts, this study supports the theory by Daniels and Turner since the derived formula seemingly predicts the total diffusion of transmembrane proteins in curved membranes accurately.

The examination of the anomalous exponents shows that the curvature has very little effect on the anomalous nature of diffusion, while the crowding effects are very similar to the planar membranes, as shown by Table 6.3 and the plots in the appendix A. There is also no noticeable difference between the anomalous diffusion exponents between the radial and longitudinal diffusion. Therefore, the curvature does not seem to interfere with the already established anomalous diffusion induced by crowding. It appears that the curvature mediated anomalous diffusion is the strongest in the longitudinal direction in small tubes particularly for lipids at displacement times shorter than 100 nanoseconds. This effect is very faint in the pure lipid tube with 10-nanometer radius, but already noticeable in dilute protein concentrations at short displacement times. However, after a few hundred nanoseconds



**Figure 6.5** Two-dimensional diffusion coefficients of proteins and lipids in systems of varying crowdedness as a function of the inverse of the radius of curvature. The planar data have been PBC corrected. For proteins, the formula for diffusion in curved membranes derived by Daniels and Turner has been fitted to the data (dashed line). For the system with 200:1 lipid to protein ratio, the obtained dynamic membrane viscosity is 0.10 Pas and for 75:1 0.18 Pas. The lipid data have been added for completeness, although the formula by Daniels and Turner is derived for larger membrane inclusions, and thus no fitting has been done.

the subdiffusion in the longitudinal direction ceases almost completely, and as a consequence, the curvature effects on anomalous diffusion appears to be weak and short-lived compared to those by crowding.



## 7 CONCLUSIONS

In this thesis, the effect of membrane curvature on the lateral diffusion of transmembrane proteins was studied for the first time with extensive molecular dynamics simulations. Numerous computational and experimental studies have focused on the dynamics in planar membranes, meanwhile, it is also known that curved membrane structures are frequent in cells, and the impact of this curvature on lateral diffusion has so far not been properly recognized. In addition, since it has been agreed that macromolecular crowding is a significant inducer of anomalous diffusion, a comparison between the effects of crowding caused by transmembrane proteins and membrane curvature was made in order to investigate whether curvature had any similar significant contributions to the anomalous diffusion.

The study was done by preparing coarse-grained simulation models of membrane tubes with a varying radius of curvature and protein crowdedness. By analyzing the diffusion motion of the lipids and proteins, it was found that while the diffusion in the longitudinal direction of the tube was mostly unaffected by the curvature, the diffusion in the radial direction experienced a significant slowdown. Protein crowding hindered the diffusion in curved membranes similarly to what has been seen with planar membranes earlier, and in the radial direction, the magnitude of the effect of nanoscale curvature was comparable to the difference in mobility between a dilute and a crowded membrane. Based on the anomalous diffusion exponents in the mean squared displacement curves of both proteins and lipids, anomalous diffusion was concluded to be mainly a result of crowding instead of membrane curvature.

Startlingly, the observed unaffected diffusion along the tube's longitudinal axis is not in line with diffusion experiments in tubular membranes. Though the systems of this thesis are smaller than what has been experimentally achievable, and this length scale difference complicates direct comparison between the simulations and experiments, the result of multiple times faster diffusion of proteins and lipids in planar membranes compared to tubes was not reproduced in this work. To investi-

gate this, the role of the shape of a protein requires focus in the future, for it has been suspected in earlier studies using planar membranes, that sterical effects such as membrane mismatch can affect transmembrane protein mobility drastically. Also, since the results between simulations and experiments for pure lipid tubes and planar membranes differ considerably, the role of lipid type and saturation also requires more elucidation. Since the hypothesis of protein shapes and lipid types being major factor in curvature dependent diffusion is easily testable, this work sparks interest in further experimentation on the mobility in curved lipid membranes.

## BIBLIOGRAPHY

- [1] K. R. Rosholm, N. Leijnse, A. Mantsiou, V. Tkach, S. L. Pedersen, V. F. Wirth, L. B. Oddershede, K. J. Jensen, K. L. Martinez, N. S. Hatzakis, *et al.*, “Membrane curvature regulates ligand-specific membrane sorting of GPCRs in living cells,” *Nature Chemical Biology*, vol. 13, no. 7, p. 724, 2017.
- [2] A. Frost, V. M. Unger, and P. De Camilli, “The BAR domain superfamily: membrane-molding macromolecules,” *Cell*, vol. 137, no. 2, pp. 191–196, 2009.
- [3] K. M. Davies, M. Strauss, B. Daum, J. H. Kief, H. D. Osiewacz, A. Rycovska, V. Zickermann, and W. Kühlbrandt, “Macromolecular organization of ATP synthase and complex I in whole mitochondria,” *Proceedings of the National Academy of Sciences*, vol. 108, no. 34, pp. 14121–14126, 2011.
- [4] J. R. Perilla, B. C. Goh, C. K. Cassidy, B. Liu, R. C. Bernardi, T. Rudack, H. Yu, Z. Wu, and K. Schulten, “Molecular dynamics simulations of large macromolecular complexes,” *Current Opinion in Structural Biology*, vol. 31, pp. 64–74, 2015.
- [5] G. Guigas and M. Weiss, “Effects of protein crowding on membrane systems,” *Biochimica et Biophysica Acta (BBA)-Biomembranes*, vol. 1858, no. 10, pp. 2441–2450, 2016.
- [6] M. R. Horton, F. Höfling, J. O. Rädler, and T. Franosch, “Development of anomalous diffusion among crowding proteins,” *Soft Matter*, vol. 6, no. 12, pp. 2648–2656, 2010.
- [7] F. Höfling and T. Franosch, “Anomalous transport in the crowded world of biological cells,” *Reports on Progress in Physics*, vol. 76, no. 4, p. 046602, 2013.
- [8] M. Javanainen, H. Hammaren, L. Monticelli, J.-H. Jeon, M. S. Miettinen, H. Martinez-Seara, R. Metzler, and I. Vattulainen, “Anomalous and normal diffusion of proteins and lipids in crowded lipid membranes,” *Faraday Discussions*, vol. 161, pp. 397–417, 2013.
- [9] B. Alberts, D. Bray, K. Hopkin, A. Johnson, J. Lewis, M. Raff, K. Roberts, and P. Walter, *Essential Cell Biology 3rd edition*. Garland Science, 2010.

- [10] M. T. Madigan, J. M. Martinko, D. A. Stahl, and D. P. Clark, *Brock Biology of Microorganisms 13th edition*. Pearson Education, Inc, 2012.
- [11] A. G. Lee, “Lipid–protein interactions in biological membranes: a structural perspective,” *Biochimica et Biophysica Acta (BBA)-Biomembranes*, vol. 1612, no. 1, pp. 1–40, 2003.
- [12] M. Manna, M. Niemelä, J. Tynkkynen, M. Javanainen, W. Kulig, D. J. Müller, T. Róg, and I. Vattulainen, “Mechanism of allosteric regulation of  $\beta$ 2-adrenergic receptor by cholesterol,” *eLife*, vol. 5, p. e18432, 2016.
- [13] M. Javanainen, G. Enkavi, R. Guixà-González, W. Kulig, H. Martinez-Seara, I. Levental, and I. Vattulainen, “Reduced level of docosahexaenoic acid shifts GPCR neuroreceptors to less ordered membrane regions,” *PLoS Computational Biology*, vol. 15, no. 5, p. e1007033, 2019.
- [14] K. Simons and E. Ikonen, “Functional rafts in cell membranes,” *Nature*, vol. 387, no. 6633, p. 569, 1997.
- [15] G. Van Meer, D. R. Voelker, and G. W. Feigenson, “Membrane lipids: where they are and how they behave,” *Nature Reviews Molecular Cell Biology*, vol. 9, no. 2, p. 112, 2008.
- [16] T. Harayama and H. Riezman, “Understanding the diversity of membrane lipid composition,” *Nature Reviews Molecular Cell Biology*, 2018.
- [17] J. T. Mika and B. Poolman, “Macromolecule diffusion and confinement in prokaryotic cells,” *Current Opinion in Biotechnology*, vol. 22, no. 1, pp. 117–126, 2011.
- [18] R. Peters and R. J. Cherry, “Lateral and rotational diffusion of bacteriorhodopsin in lipid bilayers: experimental test of the Saffman-Delbrück equations,” *Proceedings of the National Academy of Sciences*, vol. 79, no. 14, pp. 4317–4321, 1982.
- [19] W. L. C. Vaz, F. Goodsaid-Zalduondo, and K. Jacobson, “Lateral diffusion of lipids and proteins in bilayer membranes,” *FEBS Letters*, vol. 174, no. 2, pp. 199–207, 1984.
- [20] M. J. Saxton, “Lateral diffusion in an archipelago. the effect of mobile obstacles,” *Biophysical Journal*, vol. 52, no. 6, pp. 989–997, 1987.

- [21] A. P. Minton, “Macromolecular crowding and molecular recognition,” *Journal of Molecular Recognition*, vol. 6, no. 4, pp. 211–214, 1993.
- [22] P. F. F. Almeida and W. L. C. Vaz, “Lateral diffusion in membranes,” *Handbook of Biological Physics*, vol. 1, pp. 305–357, 1995.
- [23] I. Casuso, J. Khao, M. Chami, P. Paul-Gilloteaux, M. Husain, J.-P. Duneau, H. Stahlberg, J. N. Sturgis, and S. Scheuring, “Characterization of the motion of membrane proteins using high-speed atomic force microscopy,” *Nature Nanotechnology*, vol. 7, no. 8, p. 525, 2012.
- [24] N. Oppenheimer and H. Diamant, “Correlated diffusion of membrane proteins and their effect on membrane viscosity,” *Biophysical Journal*, vol. 96, no. 8, pp. 3041–3049, 2009.
- [25] J. E. Goose and M. S. P. Sansom, “Reduced lateral mobility of lipids and proteins in crowded membranes,” *PLoS Computational Biology*, vol. 9, no. 4, p. e1003033, 2013.
- [26] G. Guigas and M. Weiss, “Membrane protein mobility depends on the length of extra-membrane domains and on the protein concentration,” *Soft Matter*, vol. 11, no. 1, pp. 33–37, 2015.
- [27] J.-H. Jeon, M. Javanainen, H. Martinez-Seara, R. Metzler, and I. Vattulainen, “Protein crowding in lipid bilayers gives rise to non-Gaussian anomalous lateral diffusion of phospholipids and proteins,” *Physical Review X*, vol. 6, no. 2, p. 021006, 2016.
- [28] M. Javanainen, H. Martinez-Seara, R. Metzler, and I. Vattulainen, “Diffusion of integral membrane proteins in protein-rich membranes,” *The Journal of Physical Chemistry Letters*, vol. 8, no. 17, pp. 4308–4313, 2017.
- [29] H. T. McMahon and J. L. Gallop, “Membrane curvature and mechanisms of dynamic cell membrane remodelling,” *Nature*, vol. 438, no. 7068, p. 590, 2005.
- [30] G. A. Korn and T. M. Korn, *Mathematical handbook for scientists and engineers: definitions, theorems, and formulas for reference and review*. Courier Corporation, 2000.
- [31] J. Zimmerberg and M. M. Kozlov, “How proteins produce cellular membrane curvature,” *Nature Reviews Molecular Cell Biology*, vol. 7, no. 1, pp. 9–19, 2006.

- [32] R. M. Bhaskara, P. Grumati, J. Garcia-Pardo, S. Kalayil, A. Covarrubias-Pinto, W. Chen, M. Kudryashev, I. Dikic, and G. Hummer, “Curvature induction and membrane remodeling by FAM134B reticulon homology domain assist selective ER-phagy,” *Nature Communications*, vol. 10, no. 1, p. 2370, 2019.
- [33] H. H. Mollenhauer and D. J. Morr e, “The tubular network of the Golgi apparatus,” *Histochemistry and Cell Biology*, vol. 109, no. 5-6, pp. 533–543, 1998.
- [34] C. Lee and L. B. Chen, “Dynamic behavior of endoplasmic reticulum in living cells,” *Cell*, vol. 54, no. 1, pp. 37–46, 1988.
- [35] C. J. S. Klaus, K. Raghunathan, E. DiBenedetto, and A. K. Kenworthy, “Analysis of diffusion in curved surfaces and its application to tubular membranes,” *Molecular Biology of the Cell*, vol. 27, no. 24, pp. 3937–3946, 2016.
- [36] J. B. Hursh, “Conduction velocity and diameter of nerve fibers,” *American Journal of Physiology-Legacy Content*, vol. 127, no. 1, pp. 131–139, 1939.
- [37] G. van Meer and W. L. C. Vaz, “Membrane curvature sorts lipids,” *EMBO Reports*, vol. 6, no. 5, pp. 418–419, 2005.
- [38] M. Przybylo, J. S ykor a, J. Humpol ickov a, A. Benda, A. Zan, and M. Hof, “Lipid diffusion in giant unilamellar vesicles is more than 2 times faster than in supported phospholipid bilayers under identical conditions,” *Langmuir*, vol. 22, no. 22, pp. 9096–9099, 2006.
- [39] M. L. Henle and A. J. Levine, “Hydrodynamics in curved membranes: The effect of geometry on particulate mobility,” *Physical Review E*, vol. 81, no. 1, p. 011905, 2010.
- [40] D. R. Daniels and M. S. Turner, “Diffusion on membrane tubes: a highly discriminatory test of the Saffman–Delbruck theory,” *Langmuir*, vol. 23, no. 12, pp. 6667–6670, 2007.
- [41] Y. A. Domanov, S. Aimon, G. E. S. Toombes, M. Renner, F. Quemeneur, A. Triller, M. S. Turner, and P. Bassereau, “Mobility in geometrically confined membranes,” *Proceedings of the National Academy of Sciences*, vol. 108, no. 31, pp. 12605–12610, 2011.

- [42] M. Renner, Y. Domanov, F. Sandrin, I. Izeddin, P. Bassereau, and A. Triller, “Lateral diffusion on tubular membranes: quantification of measurements bias,” *PLoS One*, vol. 6, no. 9, p. e25731, 2011.
- [43] C. Campillo, P. Sens, D. Köster, L.-L. Pontani, D. Lévy, P. Bassereau, P. Nassoy, and C. Sykes, “Unexpected membrane dynamics unveiled by membrane nanotube extrusion,” *Biophysical Journal*, vol. 104, no. 6, pp. 1248–1256, 2013.
- [44] S. Aimon, A. Callan-Jones, A. Berthaud, M. Pinot, G. E. S. Toombes, and P. Bassereau, “Membrane shape modulates transmembrane protein distribution,” *Developmental Cell*, vol. 28, no. 2, pp. 212–218, 2014.
- [45] F. Quemeneur, J. K. Sigurdsson, M. Renner, P. J. Atzberger, P. Bassereau, and D. Lacoste, “Shape matters in protein mobility within membranes,” *Proceedings of the National Academy of Sciences*, vol. 111, no. 14, pp. 5083–5087, 2014.
- [46] T. B. Blum, A. Hahn, T. Meier, K. M. Davies, and W. Kühlbrandt, “Dimers of mitochondrial ATP synthase induce membrane curvature and self-assemble into rows,” *Proceedings of the National Academy of Sciences*, vol. 116, no. 10, pp. 4250–4255, 2019.
- [47] P. C. Nelson, *Biological Physics, energy, information, life*. W. H. Freeman and Company, 2008.
- [48] A. Einstein, “Über die von der molekularkinetischen Theorie der Wärme geforderte Bewegung von in ruhenden Flüssigkeiten suspendierten Teilchen,” *Annalen der Physik*, vol. 322, no. 8, pp. 549–560, 1905.
- [49] A. Einstein, “Zur Theorie der Brownschen Bewegung,” *Annalen der Physik*, vol. 324, no. 2, pp. 371–381, 1906.
- [50] R. Metzler, J.-H. Jeon, A. G. Cherstvy, and E. Barkai, “Anomalous diffusion models and their properties: non-stationarity, non-ergodicity, and ageing at the centenary of single particle tracking,” *Physical Chemistry Chemical Physics*, vol. 16, no. 44, pp. 24128–24164, 2014.
- [51] R. J. Ellis, “Macromolecular crowding: obvious but underappreciated,” *Trends in Biochemical Sciences*, vol. 26, no. 10, pp. 597–604, 2001.

- [52] R. J. Ellis, “Macromolecular crowding: an important but neglected aspect of the intracellular environment,” *Current Opinion in Structural Biology*, vol. 11, no. 1, pp. 114–119, 2001.
- [53] L. F. Richardson, “Atmospheric diffusion shown on a distance-neighbour graph,” *Proceedings of the Royal Society of London. Series A, Containing Papers of a Mathematical and Physical Character*, vol. 110, no. 756, pp. 709–737, 1926.
- [54] M. J. Saxton, “Anomalous diffusion due to obstacles: a Monte Carlo study,” *Biophysical Journal*, vol. 66, no. 2, pp. 394–401, 1994.
- [55] S. Chiantia, J. Ries, and P. Schuille, “Fluorescence correlation spectroscopy in membrane structure elucidation,” *Biochimica et Biophysica Acta (BBA)-Biomembranes*, vol. 1788, no. 1, pp. 225–233, 2009.
- [56] E. Flenner, J. Das, M. C. Rheinstädter, and I. Kosztin, “Subdiffusion and lateral diffusion coefficient of lipid atoms and molecules in phospholipid bilayers,” *Physical Review E*, vol. 79, no. 1, p. 011907, 2009.
- [57] J.-H. Jeon, H. Martinez-Seara, M. Javanainen, and R. Metzler, “Anomalous diffusion of phospholipids and cholesterol in a lipid bilayer and its origins,” *Physical Review Letters*, vol. 109, no. 18, p. 188103, 2012.
- [58] D. Krapf, “Mechanisms underlying anomalous diffusion in the plasma membrane,” in *Current Topics in Membranes*, vol. 75, pp. 167–207, Elsevier, 2015.
- [59] E. P. Carpenter, K. Beis, A. D. Cameron, and S. Iwata, “Overcoming the challenges of membrane protein crystallography,” *Current Opinion in Structural Biology*, vol. 18, no. 5, pp. 581–586, 2008.
- [60] P. G. Saffman and M. Delbrück, “Brownian motion in biological membranes,” *Proceedings of the National Academy of Sciences*, vol. 72, no. 8, pp. 3111–3113, 1975.
- [61] P. G. Saffman, “Brownian motion in thin sheets of viscous fluid,” *Journal of Fluid Mechanics*, vol. 73, no. 4, pp. 593–602, 1976.



- [62] W. L. C. Vaz, M. Criado, V. M. C. Madeira, G. Schoellmann, and T. M. Jovin, "Size dependence of the translational diffusion of large integral membrane proteins in liquid-crystalline phase lipid bilayers. a study using fluorescence recovery after photobleaching," *Biochemistry*, vol. 21, no. 22, pp. 5608–5612, 1982.
- [63] W. L. Vaz, F. Goodsaid-Zalduondo, and K. Jacobson, "Lateral diffusion of lipids and proteins in bilayer membranes," *FEBS Letters*, vol. 174, no. 2, pp. 199–207, 1984.
- [64] S. J. Bussell, D. L. Koch, and D. A. Hammer, "Effect of hydrodynamic interactions on the diffusion of integral membrane proteins: tracer diffusion in organelle and reconstituted membranes," *Biophysical Journal*, vol. 68, no. 5, pp. 1828–1835, 1995.
- [65] S. J. Bussell, D. L. Koch, and D. A. Hammer, "Effect of hydrodynamic interactions on the diffusion of integral membrane proteins: diffusion in plasma membranes," *Biophysical Journal*, vol. 68, no. 5, pp. 1836–1849, 1995.
- [66] Y. Gambin, R. Lopez-Esparza, M. Reffay, E. Sieracki, N. S. Gov, M. H. R. S. Genest, R. S. Hodges, and W. Urbach, "Lateral mobility of proteins in liquid membranes revisited," *Proceedings of the National Academy of Sciences*, vol. 103, no. 7, pp. 2098–2102, 2006.
- [67] J. Kriegsmann, I. Gregor, I. Von der Hocht, J. Klare, M. Engelhard, J. Enderlein, and J. Fitter, "Translational diffusion and interaction of a photoreceptor and its cognate transducer observed in giant unilamellar vesicles by using dual-focus FCS," *ChemBioChem*, vol. 10, no. 11, pp. 1823–1829, 2009.
- [68] G. Guigas and M. Weiss, "Size-dependent diffusion of membrane inclusions," *Biophysical Journal*, vol. 91, no. 7, pp. 2393–2398, 2006.
- [69] A. Naji, A. J. Levine, and P. A. Pincus, "Corrections to the Saffman-Delbrück mobility for membrane bound proteins," *Biophysical Journal*, vol. 93, no. 11, pp. L49–L51, 2007.
- [70] B. D. Hughes, B. A. Pailthorpe, and L. R. White, "The translational and rotational drag on a cylinder moving in a membrane," *Journal of Fluid Mechanics*, vol. 110, pp. 349–372, 1981.

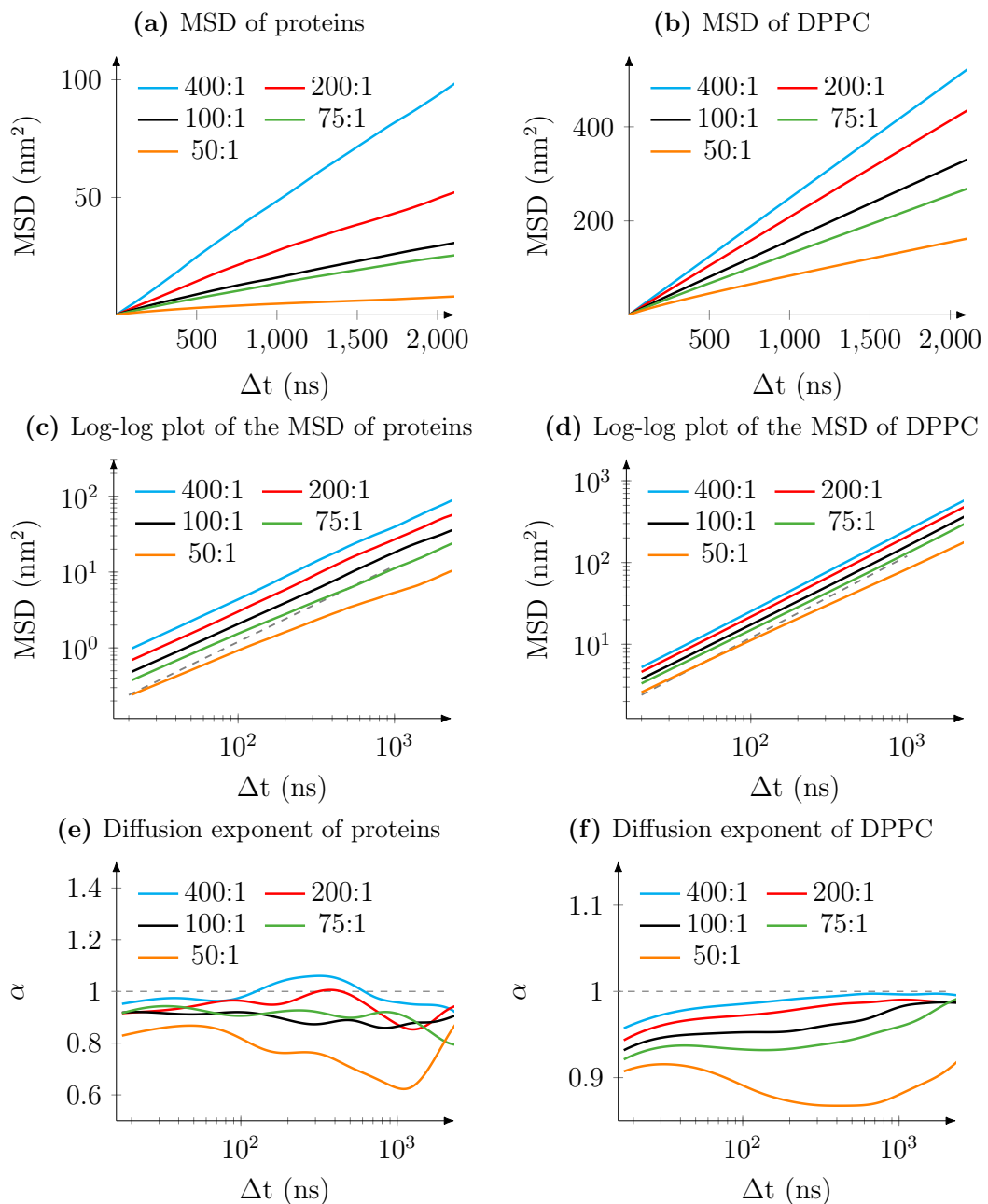
- [71] E. P. Petrov and P. Schwille, “Translational diffusion in lipid membranes beyond the Saffman-Delbrück approximation,” *Biophysical Journal*, vol. 94, no. 5, pp. L41–L43, 2008.
- [72] G. Guigas and M. Weiss, “Influence of hydrophobic mismatching on membrane protein diffusion,” *Biophysical Journal*, vol. 95, no. 3, pp. L25–L27, 2008.
- [73] S. Ramadurai, A. Holt, V. Krasnikov, G. van den Bogaart, J. A. Killian, and B. Poolman, “Lateral diffusion of membrane proteins,” *Journal of the American Chemical Society*, vol. 131, no. 35, pp. 12650–12656, 2009.
- [74] S. Ramadurai, R. Duurkens, V. V. Krasnikov, and B. Poolman, “Lateral diffusion of membrane proteins: consequences of hydrophobic mismatch and lipid composition,” *Biophysical Journal*, vol. 99, no. 5, pp. 1482–1489, 2010.
- [75] K. Weiß, A. Neef, Q. Van, S. Kramer, I. Gregor, and J. Enderlein, “Quantifying the diffusion of membrane proteins and peptides in black lipid membranes with 2-focus fluorescence correlation spectroscopy,” *Biophysical Journal*, vol. 105, no. 2, pp. 455–462, 2013.
- [76] A. K. Sharma, *Text book of differential calculus*. Discovery publishing house, 2004.
- [77] S. Pall, M. J. Abraham, C. Kutzner, B. Hess, and E. Lindahl, “Tackling exascale software challenges in molecular dynamics simulations with GROMACS,” in *International Conference on Exascale Applications and Software*, pp. 3–27, Springer, 2014.
- [78] D. van de Spoel, E. Lindahl, B. Hess, and the GROMACS development team, “GROMACS user manual version 4.6.3.” [www.gromacs.org](http://www.gromacs.org). accessed 18-November-2013.
- [79] J. Gorzynski Smith, *Organic Chemistry 2nd edition*. The McGraw-Hill Companies, 2008.
- [80] S. J. Marrink, A. H. De Vries, and A. E. Mark, “Coarse grained model for semi-quantitative lipid simulations,” *The Journal of Physical Chemistry B*, vol. 108, no. 2, pp. 750–760, 2004.

- [81] S. J. Marrink, H. J. Risselada, S. Yefimov, D. P. Tieleman, and A. H. De Vries, “The MARTINI force field: coarse grained model for biomolecular simulations,” *The Journal of Physical Chemistry B*, vol. 111, no. 27, pp. 7812–7824, 2007.
- [82] L. Monticelli, S. K. Kandasamy, X. Periole, R. G. Larson, D. P. Tieleman, and S. J. Marrink, “The MARTINI coarse-grained force field: extension to proteins,” *Journal of Chemical Theory and Computation*, vol. 4, no. 5, pp. 819–834, 2008.
- [83] D. H. de Jong, G. Singh, W. F. D. Bennett, C. Arnarez, T. A. Wassenaar, L. V. Schäfer, X. Periole, D. P. Tieleman, and S. J. Marrink, “Improved parameters for the MARTINI coarse-grained protein force field,” *Journal of Chemical Theory and Computation*, vol. 9, no. 1, pp. 687–697, 2012.
- [84] M. Javanainen, H. Martinez-Seara, and I. Vattulainen, “Excessive aggregation of membrane proteins in the martini model,” *PLoS One*, vol. 12, no. 11, p. e0187936, 2017.
- [85] A. C. Stark, C. T. Andrews, and A. H. Elcock, “Toward optimized potential functions for protein–protein interactions in aqueous solutions: osmotic second virial coefficient calculations using the martini coarse-grained force field,” *Journal of Chemical Theory and Computation*, vol. 9, no. 9, pp. 4176–4185, 2013.
- [86] R. Baron, D. Trzesniak, A. H. de Vries, A. Elsener, S. J. Marrink, and W. F. van Gunsteren, “Comparison of thermodynamic properties of coarse-grained and atomic-level simulation models,” *ChemPhysChem*, vol. 8, no. 3, pp. 452–461, 2007.
- [87] B. Hess, H. Bekker, H. J. C. Berendsen, J. G. E. M. Fraaije, *et al.*, “LINCS: a linear constraint solver for molecular simulations,” *Journal of Computational Chemistry*, pp. 1463–1472, 1997.
- [88] D. L. Evans and B. L. Holian, “The Nosé–Hoover thermostat,” *The Journal of Chemical Physics*, pp. 4069–4074, 1985.
- [89] R. Martoňák, A. Laio, and M. Parrinello, “Predicting crystal structures: the Parrinello-Rahman method revisited,” *Physical Review Letters*, p. 075503, 2003.

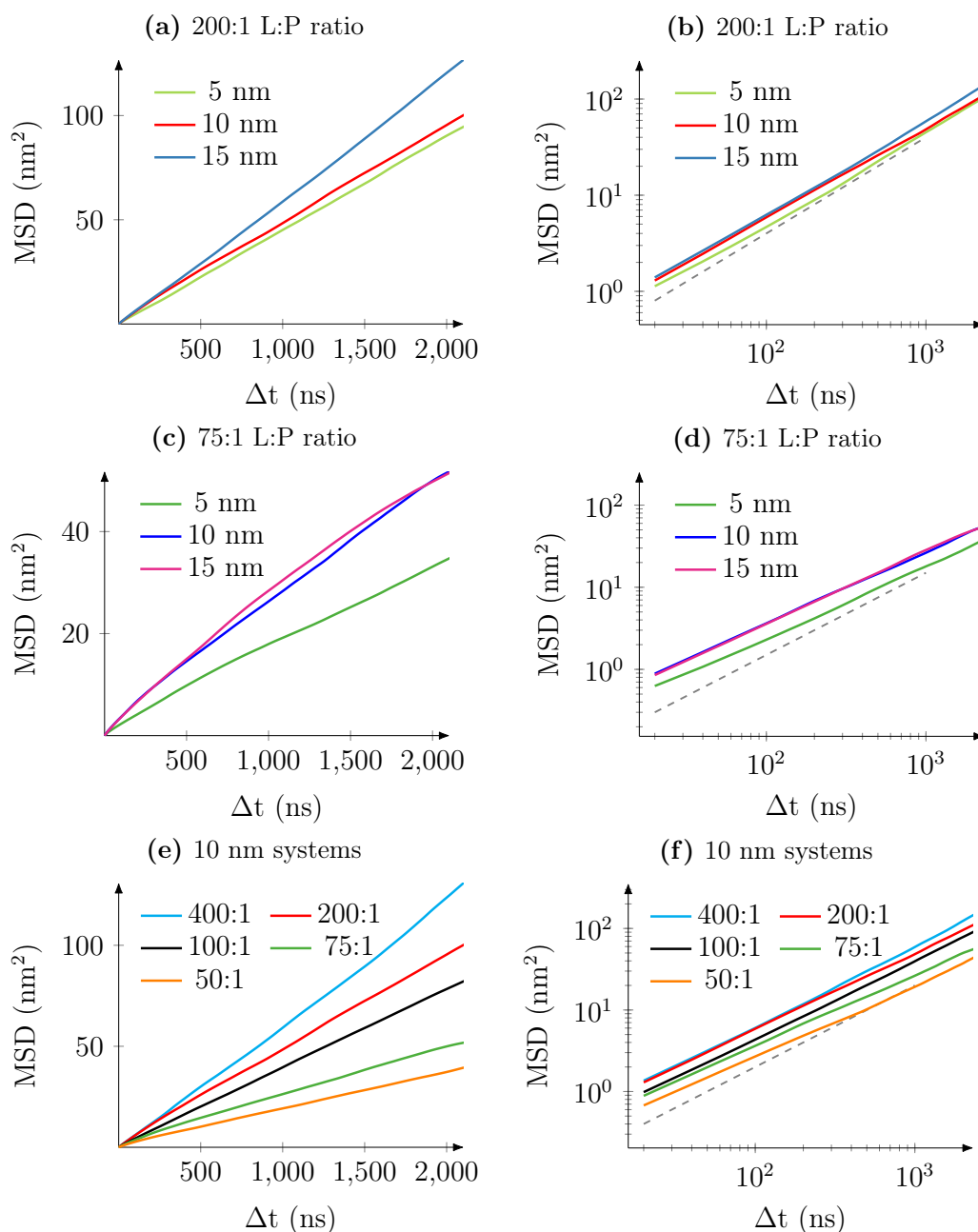
- [90] I.-C. Yeh and G. Hummer, “System-size dependence of diffusion coefficients and viscosities from molecular dynamics simulations with periodic boundary conditions,” *The Journal of Physical Chemistry B*, vol. 108, no. 40, pp. 15873–15879, 2004.
- [91] B. A. Camley, M. G. Lerner, R. W. Pastor, and F. L. H. Brown, “Strong influence of periodic boundary conditions on lateral diffusion in lipid bilayer membranes,” *The Journal of Chemical Physics*, vol. 143, no. 24, p. 12B604\_1, 2015.
- [92] M. Vögele and G. Hummer, “Divergent diffusion coefficients in simulations of fluids and lipid membranes,” *The Journal of Physical Chemistry B*, vol. 120, no. 33, pp. 8722–8732, 2016.
- [93] M. Linke, J. Koöfinger, and G. Hummer, “Rotational diffusion depends on box size in molecular dynamics simulations,” *The Journal of Physical Chemistry Letters*, vol. 9, no. 11, pp. 2874–2878, 2018.
- [94] R. M. Venable, H. I. Ingólfsson, M. G. Lerner, B. S. Perrin Jr, B. A. Camley, S. J. Marrink, F. L. H. Brown, and R. W. Pastor, “Lipid and peptide diffusion in bilayers: The Saffman–Delbrück model and periodic boundary conditions,” *The Journal of Physical Chemistry B*, vol. 121, no. 15, pp. 3443–3457, 2017.
- [95] G. V. Subbarao and B. van den Berg, “Crystal structure of the monomeric porin OmpG,” *Journal of Molecular Biology*, vol. 360, no. 4, pp. 750–759, 2006.
- [96] H. M. Berman, J. Westbrook, Z. Feng, G. Gilliland, T. N. Bhat, H. Weissig, I. N. Shindyalov, and P. E. Bourne, “The protein data bank,” *Nucleic Acids Research*, vol. 28, no. 1, pp. 235–242, 2000.
- [97] H. Berman, K. Henrick, and H. Nakamura, “Announcing the worldwide protein data bank,” *Nature Structural & Molecular Biology*, vol. 10, no. 12, pp. 980–980, 2003.
- [98] H. M. Berman, J. Westbrook, Z. Feng, G. Gilliland, T. N. Bhat, H. Weissig, I. N. Shindyalov, and P. E. Bourne, “The protein data bank.” <http://www.rcsb.org/pdb/home/home.do>. accessed 18-November-2013.

- [99] L. Martínez, R. Andrade, E. G. Birgin, and J. M. Martínez, “PACKMOL: a package for building initial configurations for molecular dynamics simulations,” *Journal of Computational Chemistry*, vol. 30, no. 13, pp. 2157–2164, 2009.
- [100] W. Humphrey, A. Dalke, and K. Schulten, “VMD - Visual molecular dynamics,” *Journal of Molecular Graphics*, pp. 33–38, 1996.
- [101] W. K. den Otter and S. A. Shkulipa, “Intermonolayer friction and surface shear viscosity of lipid bilayer membranes,” *Biophysical Journal*, vol. 93, no. 2, pp. 423–433, 2007.
- [102] A. A. Gurtovenko, M. Javanainen, F. Lolicato, and I. Vattulainen, “The devil is in the details: what do we really track in single-particle tracking experiments of diffusion in biological membranes?,” *The Journal of Physical Chemistry Letters*, vol. 10, no. 5, pp. 1005–1011, 2019.
- [103] M. Vögele, J. Köfinger, and G. Hummer, “Hydrodynamics of diffusion in lipid membrane simulations,” *Physical Review Letters*, vol. 120, no. 26, p. 268104, 2018.
- [104] S. Baoukina, S. J. Marrink, and D. P. Tieleman, “Molecular structure of membrane tethers,” *Biophysical Journal*, vol. 102, no. 8, pp. 1866–1871, 2012.

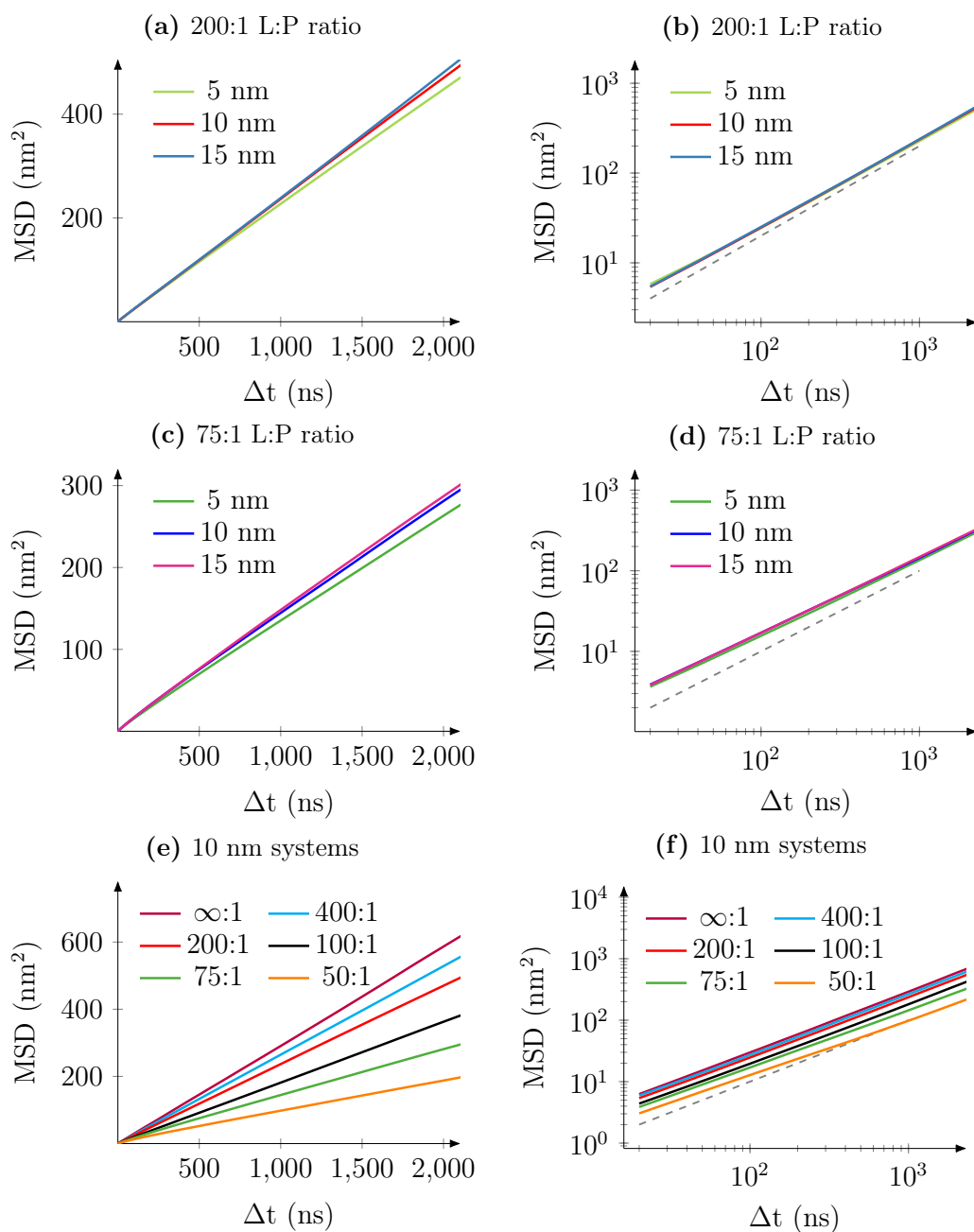
## APPENDIX A: MSD AND ANOMALOUS EXPONENTS



**Figure 7.1** Diffusion in planar membranes. Figures 7.1a and 7.1b show the MSD of the proteins and lipids respectively. In plots 7.1c and 7.1d, the MSD has been plotted on a log-log axis, along with a dashed line indicating normal diffusion. All of the  $2 \mu\text{s}$  of data plotted in the graphs have been used for the diffusion coefficient fitting. Figures 7.1e and 7.1f show the evolution of the diffusion exponents of proteins and lipids on a semi-log axis.

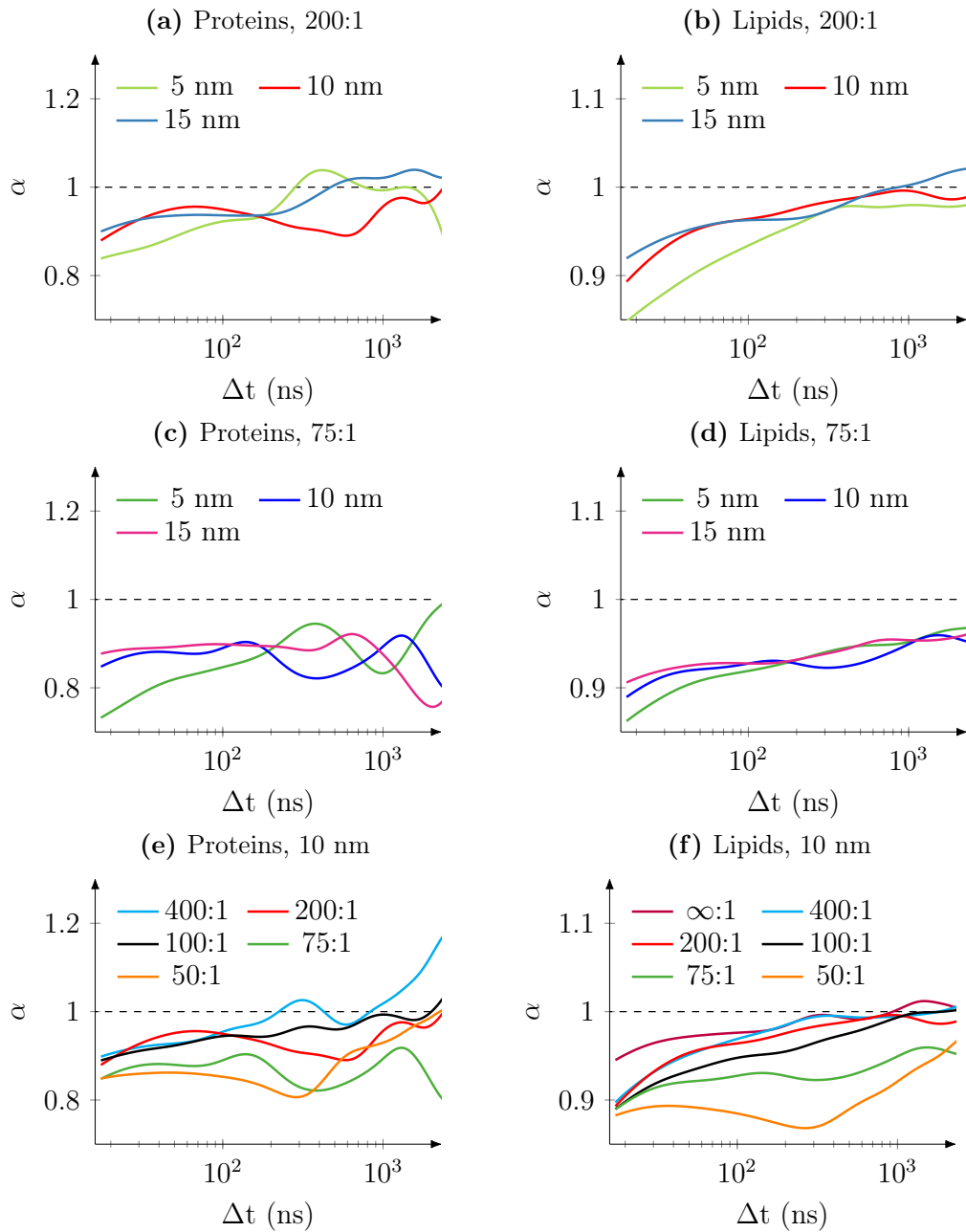


**Figure 7.2** Mean squared displacement of proteins in tubular membranes. In Figures 7.2a, 7.2b, 7.2c, and 7.2d, the MSD data of proteins in tubes of varying radii and with lipid to protein ratios of 200:1 and 75:1 are shown in normal and log-log plots. In Figures 7.2e and 7.2f, the MSD data is plotted for 10 nm systems with varying crowdedness in a normal and a log-log plot. All of the 2  $\mu\text{s}$  of data plotted in the graphs have been used for the fitting of the MSD diffusion law.

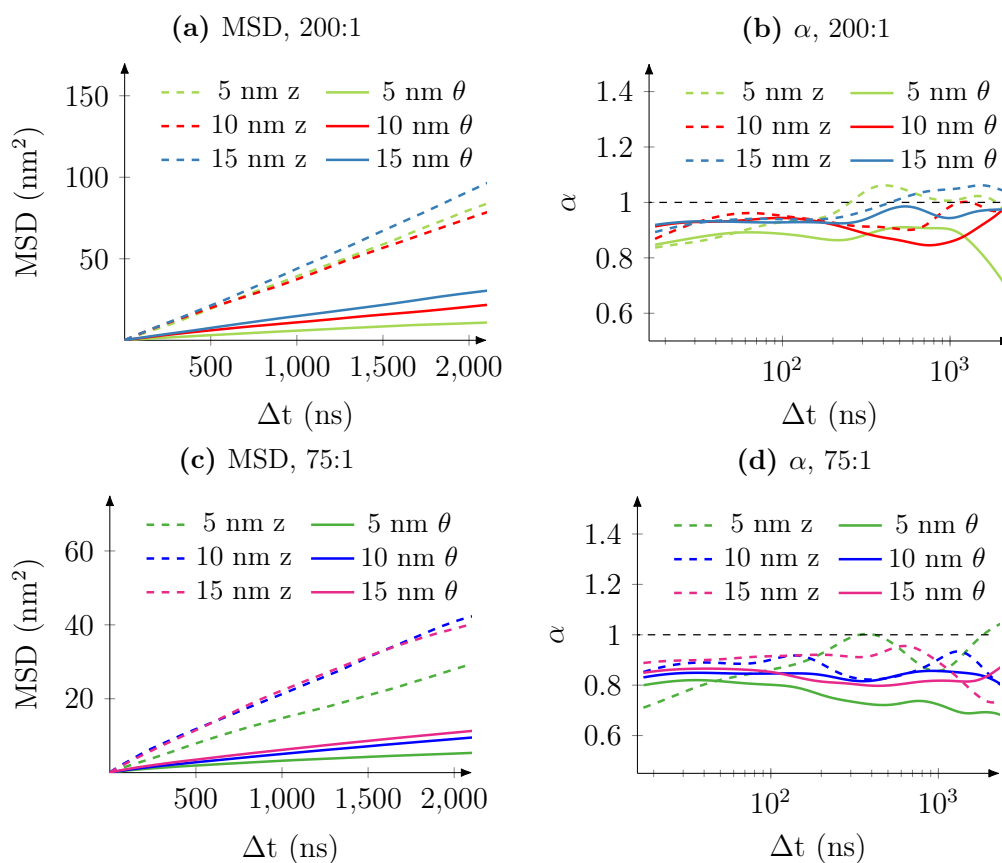


**Figure 7.3** Similarly to Figure 7.2, the diffusion of lipids is plotted in normal and log-log plot for systems with varying crowdedness and tube radius.

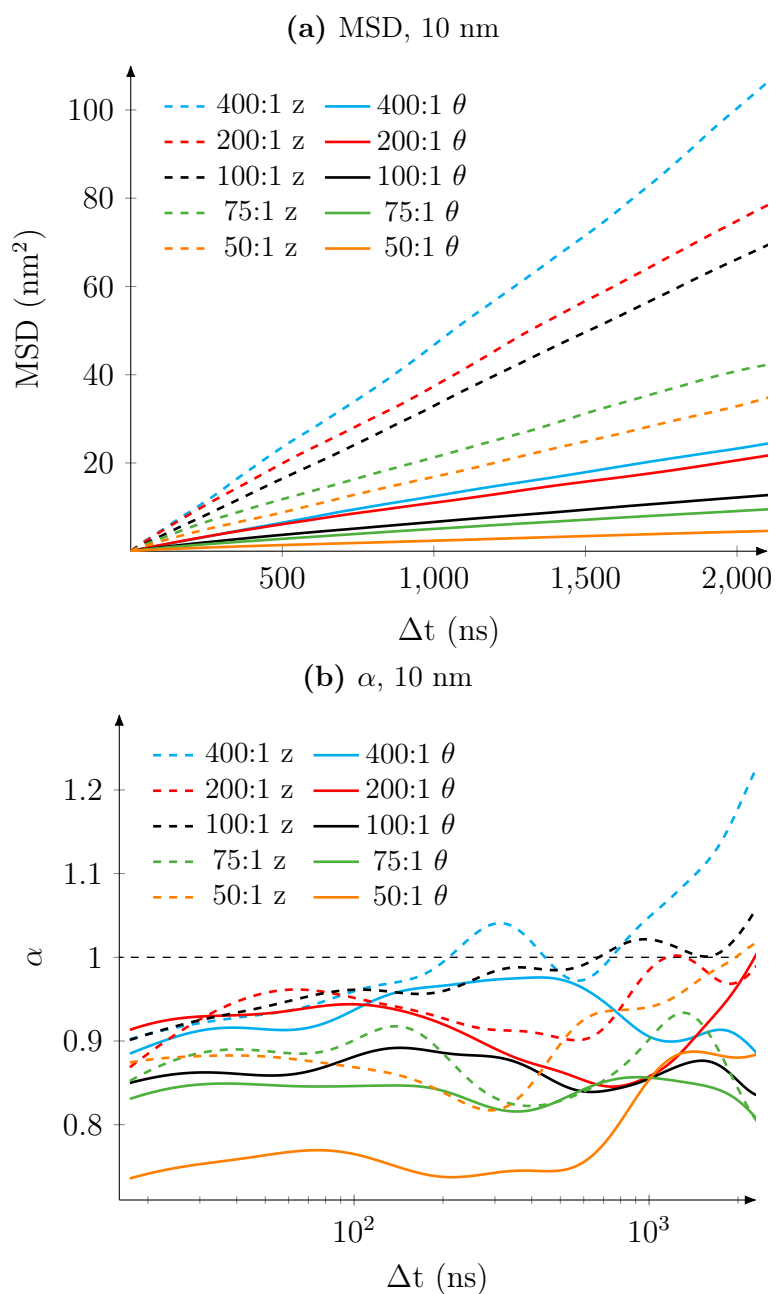




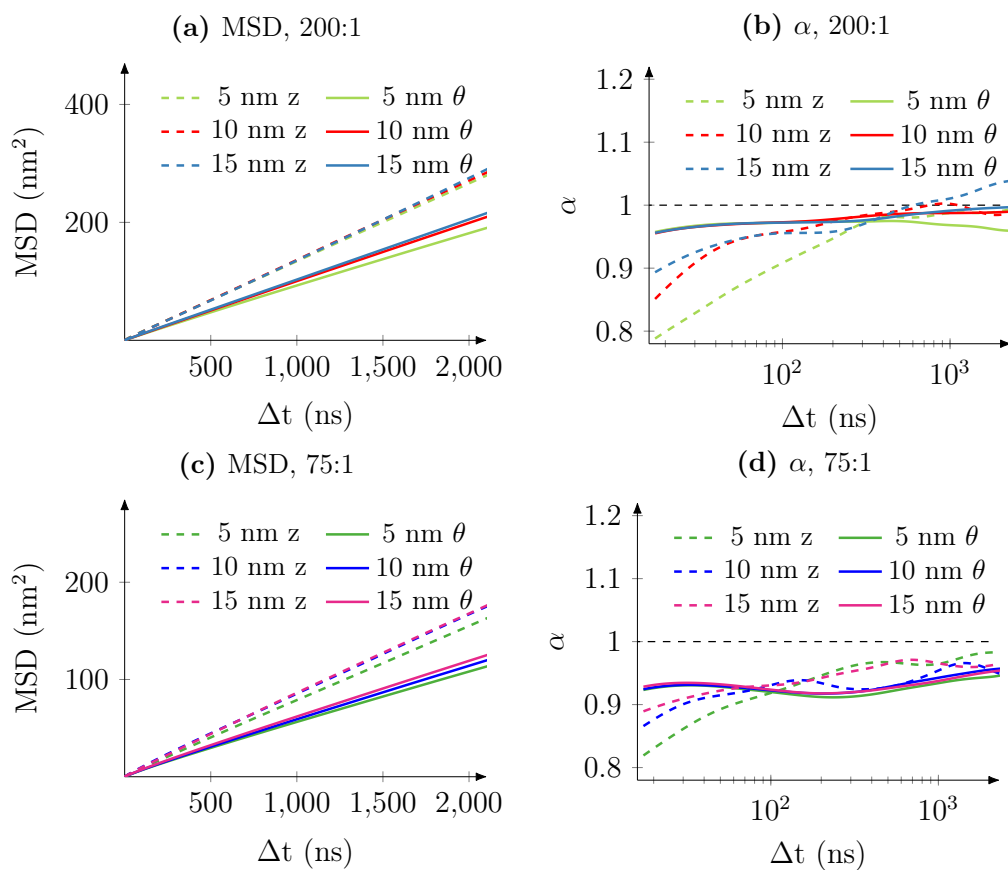
**Figure 7.4** Diffusion exponents of proteins and lipids in tubular membranes. Protein diffusion exponents are plotted on the left hand side and lipid diffusion exponents on the right. Plots have been made separately for systems with both 200:1 (7.4a 7.4b) and 75:1 (7.4c 7.4d) lipid to protein ratio, as well as for systems with 10 nm tube radius (7.4e 7.4f).



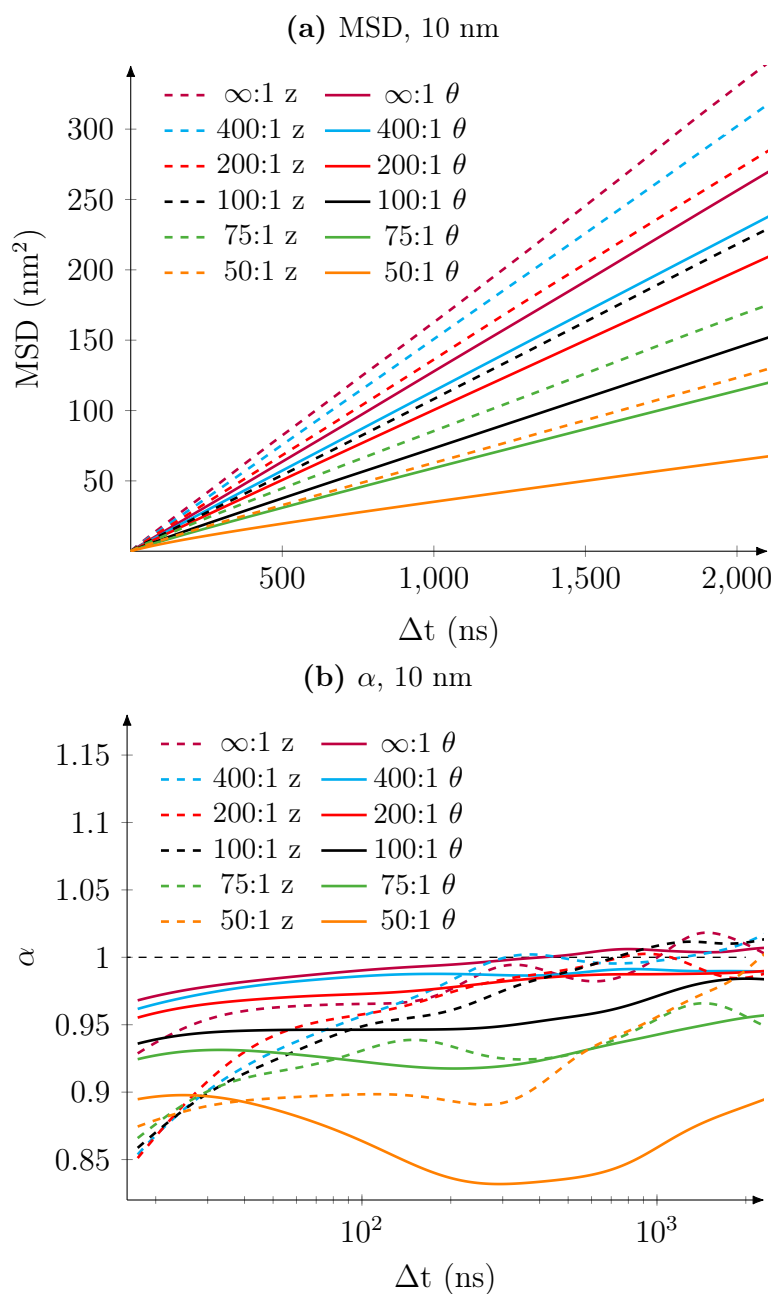
**Figure 7.5** Diffusion of proteins in tubular membranes of varying radii separated in radial and longitudinal dimensions. The MSD and diffusion exponent for systems with 200:1 lipid to protein ratio have been plotted in Figures 7.5a and 7.5b and the same for 75:1 in Figures 7.5c and 7.5d.



**Figure 7.6** Diffusion of proteins in tubular membranes of varying crowdedness separated in radial and longitudinal dimensions. The MSD of proteins in tubes with 10 nm radius has been plotted in Figure 7.6a and the diffusion exponent in Figure 7.6b.



**Figure 7.7** Similarly to the Figure 7.5, the diffusion of lipids is plotted for tubular membranes of varying radii in radial and longitudinal dimensions. The diffusion in both the systems with a 5-nanometer radius is noticeably anomalous but the effect is short-lived.



**Figure 7.8** Similarly to the Figure 7.6, the diffusion of lipids is plotted for tubular membranes of varying crowdedness in radial and longitudinal dimensions.